



# Calcium isotopic fractionation in microbially mediated gypsum precipitates

Khadouja Harouaka<sup>\*</sup>, Muammar Mansor, Jennifer L. Macalady, Matthew S. Fantle

Department of Geosciences, Penn State University, University Park, PA 16802, United States

Received 5 August 2015; accepted in revised form 3 March 2016; available online 9 March 2016

## Abstract

Gypsum ( $\text{CaSO}_4 \cdot 2\text{H}_2\text{O}$ ) precipitation experiments were carried out at low pH in the presence of the sulfur oxidizing bacterium *Acidithiobacillus thiooxidans*. The observed Ca isotopic fractionation (expressed as  $\Delta^{44/40}\text{Ca}_{\text{s-f}} = \delta^{44/40}\text{Ca}_{\text{solid}} - \delta^{44/40}\text{Ca}_{\text{fluid}}$ ) at the end of each experimental time period ( $\sim 50$  to 60 days) was  $-1.41\text{‰}$  to  $-1.09\text{‰}$  in the biotic experiments,  $-1.09\text{‰}$  in the killed control, and  $-1.01\text{‰}$  to  $-0.88\text{‰}$  in the abiotic controls. As there were no strong differences in the solution chemistry and the rate at which gypsum precipitated in the biotic and abiotic controls, we deduce a biological Ca isotope effect on the order of  $-0.3\text{‰}$ . The isotope effect correlates with a difference in crystal aspect ratios between the biotic experiments ( $8.05 \pm 3.99$ ) and abiotic controls ( $31.9 \pm 8.40$ ). We hypothesize that soluble and/or insoluble organic compounds selectively inhibit crystal growth at specific crystal faces, and that the growth inhibition affects the fractionation factor associated with gypsum precipitation. The experimental results help explain Ca isotopic variability in gypsum sampled from a sulfidic cave system, in which gypsum crystals exhibiting a diversity of morphologies (microcrystalline to cm-scale needles) have a broad range of  $\delta^{44/40}\text{Ca}$  values ( $\sim 1.2$ – $0.4\text{‰}$ ) relative to the limestone wall ( $\delta^{44/40}\text{Ca} = 1.3\text{‰}$ ). In light of the laboratory experiments, the variation in Ca isotope values in the caves can be interpreted as a consequence of gypsum precipitation in the presence of microbial organic matter and subsequent isotopic re-equilibration with the Ca source.

© 2016 Published by Elsevier Ltd.

## 1. INTRODUCTION

Over the past twenty years, calcium (Ca) isotopes have been increasingly utilized as proxies at a variety of spatial scales to inform such matters as paleo sea surface temperatures and variability in Ca cycling over a range of time scales (e.g., De La Rocha and DePaolo, 2000; DePaolo, 2004; Langer et al., 2007; Farkas et al., 2007a,b; Ewing et al., 2008; Page et al., 2008; Cenko-Tok et al., 2009; Fantle, 2010; Heuser and Eisenhauer, 2010). Notably, in both experimental and natural systems, Ca has been shown

to fractionate isotopically to a significant extent during mineral precipitation. This effect has been documented during experimental gypsum, calcite, and aragonite precipitation (Gussone et al., 2003, 2005, 2007; Lemarchand et al., 2004; Tang et al., 2008, 2011; Gussone et al., 2011; Reynard et al., 2011; Harouaka et al., 2014). Calcium isotope fractionation during mineral precipitation is believed to be kinetically controlled, and related to aqueous ion-mineral surface interactions (Fantle and DePaolo, 2007; DePaolo, 2011; Nielsen et al., 2012).

A wealth of evidence suggests that organic molecules affect the nucleation, precipitation kinetics, and morphology of Ca-rich minerals such as gypsum and calcite (e.g., Barcelona et al., 1976; Barcelona and Atwood, 1978, 1979; Cody and Cody, 1989, 1991; Cody, 1991; DeOliveira and Laursen, 1997; Hamdona and Hadad, 2008). In nature, small quantities of organic molecules are

<sup>\*</sup> Corresponding author.

E-mail addresses: [kuh121@psu.edu](mailto:kuh121@psu.edu) (K. Harouaka), [mym5203@psu.edu](mailto:mym5203@psu.edu) (M. Mansor), [jlm80@psu.edu](mailto:jlm80@psu.edu) (J.L. Macalady), [mfantle@psu.edu](mailto:mfantle@psu.edu) (M.S. Fantle).

produced abiotically (e.g., Shock, 1990), but often occur in higher abundances as a result of microbial or other biological activity (e.g., Riding and Awramik, 2000). Given the known links between microorganisms and mineral precipitation kinetics, and the relationship between the Ca isotopic composition and the precipitation kinetics of minerals, it seems both reasonable and useful to quantify Ca isotopic fractionation associated with mineral precipitation in the presence of microbes.

Microbial activity may impact the Ca isotopic composition of minerals either directly or indirectly (Fig. 1). For example, Ca plays an important role in cellular function, such that both eukaryotic and prokaryotic cells actively pump  $\text{Ca}^{2+}$  in order to maintain low intracellular  $\text{Ca}^{2+}$  concentrations ( $\sim 10^{-4}$  mM; Norris et al., 1991; Yates and Robins, 1999; Collins, 2006). Active pumping may isotopically fractionate Ca, analogous to isotopic effects observed in terrestrial ecosystems associated with plant uptake of  $\text{Ca}^{2+}$  (Skulan et al., 1997; Skulan and DePaolo, 1999; Page et al., 2008; Cenki-Tok et al., 2009; Holmden and Bélanger, 2010; Cobert et al., 2011; Farkaš et al., 2011; Schmitt et al., 2012).

Assuming that Ca isotopic effects are impacted by precipitation rate, microbial activity can also influence solution chemistry via the production of anions (e.g.,  $\text{SO}_4^{2-}$  associated with sulfur oxidation), which can increase the saturation state and, hence, the precipitation rate of minerals that contain the anion of interest in their structure (e.g.,  $\text{CaSO}_4 \cdot 2\text{H}_2\text{O}$ ). On the other hand, microbial production of dissolved organic molecules can reduce the activity of  $\text{Ca}^{2+}$  in aqueous solution via the formation of organometallic complexes, thereby decreasing saturation state and lowering precipitation rate. Lastly, microbes may sequester Ca in the process of producing extracellular polymeric substances (EPS), in which Ca is an important

structural component (e.g., Sutherland, 2001; Braissant et al., 2007; Uroz et al., 2009). Assuming EPS formation isotopically fractionates Ca, the production of biofilm could isotopically distill aqueous Ca, given a sufficient flux into the biofilm. The isotopically distilled Ca source is then reflected in the isotopic composition of contemporaneously formed minerals.

The current study investigates the Ca isotopic composition of microbially-mediated gypsum precipitates grown in the laboratory under controlled conditions, and compares the results to previously-conducted abiotic precipitation experiments. The study is motivated by the observation of significant variability in the Ca isotopic composition of gypsum collected from the sulfidic Frasassi cave system, a Mars analogue site in northern Italy (Galdenzi and Maruoka, 2003; Galdenzi, 2012; Macalady et al., 2007; Jones et al., 2008, 2011). At Frasassi, gypsum replacement crusts form via the oxidation of  $\text{H}_2\text{S}$  gas to  $\text{H}_2\text{SO}_4$ , which corrodes the limestone walls. Speleogenesis occurs in the presence of the sulfur oxidizing bacterium *Acidithiobacillus thiooxidans*, which actively drives the oxidation of  $\text{H}_2\text{S}$  (Macalady et al., 2007; Jones et al., 2008, 2011, 2015).

Accordingly, we precipitated gypsum in multiple laboratory cultures using a Ca-rich medium inoculated with *A. thiooxidans* strain GB30-2C, which oxidizes  $\text{S}^0$  to sulfuric acid ( $\text{H}_2\text{SO}_4$ ). The magnitude of Ca isotopic fractionation between the final gypsum precipitates and the final fluid ( $\Delta^{44/40}\text{Ca} = \delta^{44/40}\text{Ca}_{\text{solid}} - \delta^{44/40}\text{Ca}_{\text{fluid}}$ ) was larger in the biotic experiments than in the abiotic controls by  $\sim 0.3\%$ . The isotopic variability between biotic and control experiments was independent of solution chemistry, saturation state, and precipitation rate, yet correlated with crystal aspect ratio. This correlation suggests that the observed isotope effect may be related to surface selective interactions of organic matter with specific crystal faces. The

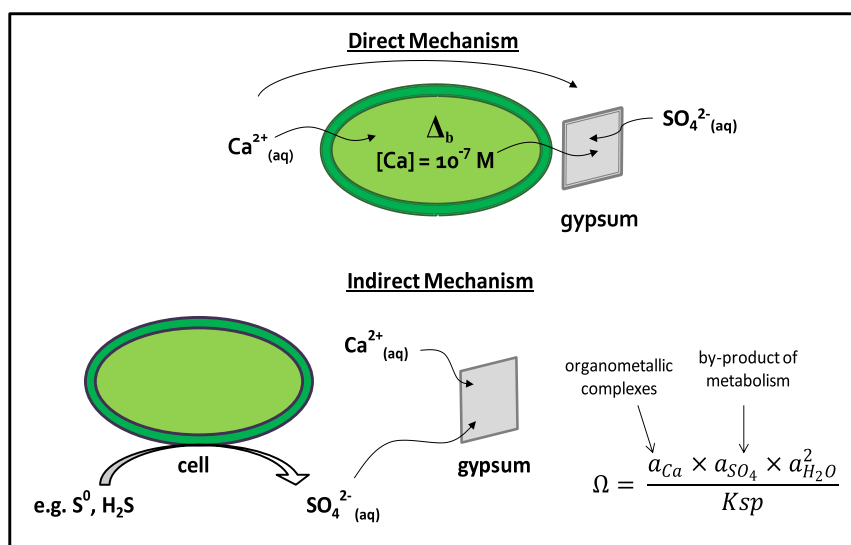


Fig. 1. Schematic of the direct and indirect pathways by which microbes could affect the Ca isotopic composition of gypsum. The pumping of Ca out of the cell is an example of a “direct” mechanism that may induce a biotic isotopic fractionation effect ( $\Delta_b$ ), which may be captured in precipitating gypsum. Changing solution chemistry (specifically mineral saturation state) due to microbial activity is an example of an indirect mechanism. An indirect mechanism can alter the kinetics of gypsum precipitation and the Ca isotopic fractionation factor associated with precipitation, and, hence, the  $\delta^{44}\text{Ca}$  of the mineral.

experimentally-constrained microbial isotope effect may help explain the  $\sim 0.8\%$  range in  $\delta^{44/40}\text{Ca}$  found in gypsum precipitates from the Frasassi cave system. The experimental results demonstrate that microbes can cause measurable Ca isotopic variations in minerals, and are therefore a plausible factor to consider in interpreting Ca isotopes in natural systems.

## 2. METHODS

### 2.1. Microbial cultures

A pure culture of *A. thiooxidans* strain GB30-2C was previously isolated from gypsum wall crusts in the Grotta Bella cavern in the Frasassi cave system (Italy) (Jones et al., 2011). Strain GB30-2C was maintained by monthly sub-culturing in liquid mineral medium containing 3 g/L  $\text{KH}_2\text{PO}_4$ , 0.5 g/L  $\text{MgSO}_4 \cdot 7\text{H}_2\text{O}$ , 0.25 g/L  $\text{CaCl}_2 \cdot 2\text{H}_2\text{O}$ , 0.2 g/L  $(\text{NH}_4)_2\text{SO}_4$ , 0.01 g/L  $\text{FeSO}_4 \cdot 7\text{H}_2\text{O}$ , which was supplemented with 1 g/L elemental sulfur ( $\text{S}^0$  sterilized by autoclaving at 100 °C for 30 min on three separate days). Cultures were incubated at room temperature on a rotary shaker. Under these conditions, strain GB30-2C produced biofilms, primarily around large sulfur particles that were oxidized to sulfate over the course of the incubation. The cells isolated in this manner were later used to inoculate the biotic gypsum precipitation experiments.

### 2.2. Biotic gypsum precipitation experiments

Gypsum was precipitated in the presence of *A. thiooxidans* strain GB30-2C with elemental sulfur as the sole source of reduced sulfur. To ensure that all sulfate was microbially-produced, the medium used to culture the microbes (Section 2.1) was modified to exclude sulfate salts, and as such  $\text{MgSO}_4 \cdot 7\text{H}_2\text{O}$  and  $(\text{NH}_4)_2\text{SO}_4$  were replaced with 0.4 g/L  $\text{MgCl}_2 \cdot 6\text{H}_2\text{O}$  and 0.08 g/L  $\text{NH}_4\text{Cl}$ , respectively. The  $\text{FeSO}_4 \cdot 7\text{H}_2\text{O}$  salt was omitted from the medium entirely. Stock media solutions were prepared with Ca concentrations of 50 and 70 mM and autoclaved. Elemental sulfur (0.1 g per culture) was placed in 125 mL PFA Erlenmeyer flasks and pre-sterilized as described above. Then 75 mL of media was added to each flask followed by 0.1 mL of cell suspension, such that the initial cell concentration of each flask was  $1 \cdot 10^5$  to  $1 \cdot 10^8$  cells/ml. The cell suspension was first diluted to the appropriate concentration, centrifuged at 8000g and resuspended twice in fresh sulfate-free medium to prevent residual sulfate from being carried over. Abiotic controls were prepared in the same manner but for excluding the addition of cells. A killed control was also prepared, where an aliquot of the cell suspension was first fixed with 3% paraformaldehyde for 2 h at 4°C. The fixed cells were centrifuged and resuspended twice in sulfate-free medium prior to being added to the flask.

The gypsum precipitation experiments were performed twice, and are therefore referred to as either “Series 1” and “Series 2”. Series 1 experiments were conducted using 50 mM  $\text{Ca}^{2+}$  media over a range of initial cell densities ( $1 \cdot 10^5$ ,  $1 \cdot 10^6$  and  $1 \cdot 10^7$  cells/ml) to assess the effect of initial bacterial abundances on gypsum precipitation and/or

isotopic systematics. Series 2 experiments were conducted using 50 mM and 70 mM  $\text{Ca}^{2+}$  media at a constant initial concentration of cells ( $1 \cdot 10^6$  cells/ml). All cultures were incubated on a shaker table (100 rpm) until gypsum precipitates were observed. Culture solutions were sampled every 2–5 days and at the termination of the experiment. Cell density in each aliquot was determined with a hemacytometer. The solution pH was measured in Series 1 using pH paper, and in Series 2 using a pH probe (Thermo Scientific 8104BNUWP). The  $\text{SO}_4^{2-}$  concentrations in all the aliquots were measured by anion chromatography (Dionex ICS-2500;  $1\text{SD} = 1.4 \text{ mM}$ ). Calcium concentration measurements of selected aliquots from each experiment were conducted by ICP-AES (PerkinElmer Optima 5300DV;  $1\text{SD} \leq 10\%$ ), and gypsum precipitation rates were constrained using the  $\text{Ca}^{2+}$  concentration data.

At the termination of each experiment, the contents of the flasks were filtered through a 0.2  $\mu\text{m}$  PVDF membrane filter. The filtrate was acidified with concentrated, ultra-pure  $\text{HNO}_3$  and set aside for Ca isotopic analysis. In order to quantify the organic content of each experiment, aliquots of the filtrate were analyzed for dissolved organic carbon (DOC; Shimadzu TOC-VCPH, using potassium hydrogen phthalate solution as a standard,  $1\text{SD} = 2 \text{ mg/L}$ ) and carbohydrate concentration measurements. The concentration of carbohydrates in the final solutions were determined via the Dubois assay (Dubois et al., 1956), in which 10  $\mu\text{L}$  of saturated phenol (EMD Omnipure UN2321) and 1 mL of concentrated  $\text{H}_2\text{SO}_4$  (EMD, 96% ACS grade) were added to 400  $\mu\text{L}$  of sample. After five minutes, absorbance was measured at 490 nm on a UV/VIS spectrophotometer (Beckman Coulter DU730). Concentration calibration curves were constructed using D-glucose (Anhydrous, Amresco) solution as a standard.

The residual gypsum and sulfur mixture was placed in benzene (Alfa Aesar 99.0% ACS grade) to dissolve the elemental sulfur, and was refiltered to recover the gypsum precipitates. The solid sample was apportioned for Ca isotope analyses, imaging by SEM (FEI Quanta 200 ESEM), and TOC measurements (Elemental Analyzer NC2500, CE Instruments; 2,5-Bis (5-tert-butyl-benzoxazol-2-yl) thiophene (BBOT) used as the standard).

To calculate precipitation rates,  $\text{Ca}^{2+}$  concentrations sampled in time were normalized to the initial concentration of the flasks prior to inoculation, and then fit via linear interpolation (Fig. C1). The precipitation rate ( $R$ ) was calculated as the average of the concentration drop ( $dC_i$ ) over a constant time interval ( $dt_i$ ) between each interpolation ( $n \sim 2000$ ):

$$R = \frac{\sum_i^n \frac{dC_i}{dt_i}}{n} \quad (1)$$

Error analysis was performed using a Monte Carlo type calculation, in which randomly generated concentration profiles were fit using linear interpolation (Fig. C2) and a precipitation rate was calculated for each iteration (Eq. (1)). The uncertainty used in the calculation was equal to the largest analytical uncertainty in the  $\text{Ca}^{2+}$  concentration measurements ( $\text{SD} = 4.8 \text{ mM}$ ), such that the reported propagated error is a maximum estimate. The reported

error in precipitation rate was calculated as the standard deviation of the rates from each iteration. The uncertainty in the calculated rates predominantly reflects uncertainty in the measured  $\text{Ca}^{2+}$  concentrations, which was impacted by limited sample volume. Precipitation rates estimated from the  $\text{Ca}^{2+}$  concentration data of Series 1 are believed to be less accurate than those of Series 2 for methodological reasons (see Section 3.1).

### 2.3. Cave sample collection

Gypsum and water samples were collected from Grotta Bella, a cave that is part of the Frasassi cave system (Italy), as well as in and around the Frasassi Gorge in June 2009 and June 2011. The gypsum precipitated adjacent to sulfidic springs that actively degas  $\text{H}_2\text{S}$ . We collected gypsum samples of four distinct morphologies (microscale crystals to large cm-length needles) from Grotta Bella in 2009. In 2011, drip waters were collected from Grotta Bella in acid-washed polypropylene bottles fitted with acid-washed funnels over a period of two to three days. In 2009, representative samples of sulfidic spring water (Fissure and Main springs; [Galdenzi and Maruoka, 2003](#)), non-sulfidic spring water (Gorgo Vivo), and Sentino River water were collected by filtering through  $0.45\ \mu\text{m}$  Acrodisc hydrophilic polypropylene (GHP) syringe filters and acidifying with ultra-pure nitric acid in the field. Temperature, conductivity, and pH were measured at each site. Two samples of Jurassic Massiccio Formation, in which the caverns are located, were collected from outcrops. The first outcrop was located at the Sentino River water sampling site and the second outcrop was near the geographic center of the Frasassi Gorge.

### 2.4. Calcium isotopic analysis (MC-ICP-MS)

Solid and fluid samples from the laboratory experiments were measured with a multi-collector inductively coupled plasma mass spectrometer at Penn State's Metal Isotope Laboratory (MIL;  $^{44}\text{Ca}/^{42}\text{Ca}$  measured on a Thermo Fisher Neptune Plus MC-ICP-MS). All samples were processed in order to remove matrix-derived isobaric interferences ([Table A1](#)), the most critical of which are those derived from trace amounts of Sr. As most of the samples measured were generated from biotic experiments, care was exercised in removing all organic carbon, which not only produces isobaric interferences (e.g.,  $^{12}\text{C}^{16}\text{O}_2$ ) but also affects the excitation efficiency of the plasma and, hence, sensitivity (e.g., [Allain et al., 1991](#); [Grindlay et al., 2006, 2013](#)).

#### 2.4.1. Sample purification

All samples (including cleaned precipitates and dried down solutions) and procedural blanks were dissolved in 6 N  $\text{HNO}_3$  and dried down. The samples were then treated twice with 30%  $\text{H}_2\text{O}_2$  to remove organic carbon. Approximately 1 mL of 30%  $\text{H}_2\text{O}_2$  was added to the sample vial containing the dried down residue, after which the vials were capped and placed on a hot plate at  $90^\circ\text{C}$  for 30 min. The vials were then uncapped and the sample was allowed to evaporate to dryness. The process was repeated a second time, after which the samples were resuspended in

4 N  $\text{HNO}_3$ . All digested sample Ca was purified using TODGA resin (Eichrome; [Horowitz et al., 2005](#); [Pourmand and Dauphas, 2010](#)) using acid-washed columns (2 cm long, 0.4 cm internal diameter). The resulting elution sequence is shown in [Table A2](#). Average column recoveries were  $96 \pm 4\%$  ([Tables A3 and A4](#)).

#### 2.4.2. Calcium isotopic analysis by MC-ICP-MS

Following column chemistry, purified samples were resuspended and diluted in 1%  $\text{HNO}_3$  to a  $\text{Ca}^{2+}$  concentration of 3 ppm, and introduced to the MC-ICP-MS as a dry aerosol using a Cetac Aridus II desolvation system with a  $100\ \mu\text{L}/\text{min}$  C-flow PFA nebulizer (RF power  $\approx 1200\ \text{W}$ ). When optimized, the Aridus effectively removes solvent-derived polyatomic interferences (e.g.,  $^{40}\text{ArH}_2^+$ ,  $^{14}\text{N}_3^+$ ,  $^{14}\text{N}_2^{16}\text{O}^+$ ) while maintaining a stable signal. A Thermo Scientific sampler Jet cone and a Spectron skimmer H cone were used, resulting in a maximum  $\sim 10\ \text{V}$   $^{44}\text{Ca}$  ion beam ( $\sim 3\ \text{ppm}$   $\text{Ca}^{2+}$  solution). Measurements were made in medium mass resolution, and ion beams at masses 48 ( $^{48}\text{Ca}^+$ ), 46 ( $^{46}\text{Ca}^+$ ), 44 ( $^{44}\text{Ca}^+$ ), 43 ( $^{43}\text{Ca}^+$ ) and 42 ( $^{42}\text{Ca}^+$ ) were monitored on the H4, H2, L1, L2, and L4 Faraday cups, respectively. The H3 cup monitors mass 47 ( $^{47}\text{Ti}^+$ ). The dominant polyatomic interferences were  $^{14}\text{N}_2^{16}\text{O}^+$  at mass 44, and  $^{40}\text{ArH}_2^+$  and  $^{14}\text{N}_3^+$  at mass 42, which had typical intensities of  $<20$ ,  $<2$ , and  $<30\ \text{mV}$ , respectively, when operating in dry plasma mode. Typical background intensities at masses 44 and 42 measured in blank 1%  $\text{HNO}_3$ , were  $<6$  and  $<2\ \text{mV}$ , respectively ([Fig. A1](#)).

Isotope ratios were collected in a single 20 cycle block, with an 8 s integration time and a 5 s idle time. Each measurement was followed by a 2 min rinse and 5 min wash in clean 1%  $\text{HNO}_3$ . Magnet stability was assessed by the relative standard deviation of each 20 cycle run ( $\text{RSD of the } 44/42 \leq 2.0 \cdot 10^{-4}$ ). Samples were measured in replicate ( $n = 3\text{--}4$ ) over multiple analytical sessions, with each sample analysis bracketed by measurements of column-purified SRM-915a (purification is made necessary by the trace Sr present in all Ca standards we investigated). The alignment of the leading edges of the various Ca-specific ion beams was assessed during the warm-up and tuning period utilizing clean 1%  $\text{HNO}_3$  and a single element tuning solution containing Ca. The plateau mass at which the Ca isotope measurement was conducted was determined via plateau tests during which the  $^{44}\text{Ca}/^{42}\text{Ca}$  ratio of SRM-915b was measured at various masses along the plateau to assess its width ( $<0.01\ \text{amu}$ ). The ideal plateau mass was approximately halfway between the plateau shoulder and the rise in ion beam intensity associated with the  $^{40}\text{ArH}_2^+$  interference ([Fig. A1](#)). The distance between the selected plateau mass and the HWFM (half width full maximum) was measured and recorded as a fixed offset parameter, and all subsequent measurements were conducted at plateau masses that were offset from the HWFM by the offset parameter. This procedure ensured that each measurement was carried out at the correct plateau position.

Instrumental mass bias is corrected using a sample-standard bracketing approach. Negligible differences were observed whether a linear, exponential, or power law was applied. Procedural blanks did not exceed maximum

background intensities (mass 44 = 6 mV, mass 42 = 2 mV). Additionally, the measurement of NIST SRM-915b and other standards, relative to SRM-915a, in each analytical session were used to assess analytical accuracy (Table 1). Though not measured extensively to date, the evolving consensus value for the difference in  $^{44}\text{Ca}/^{42}\text{Ca}$  ratio between SRM-915a and SRM-915b is 0.35‰ (see Fantle and Tipper, 2014 for a summary). On the MIL Neptune Plus, the measured difference between SRM-915a and SRM-915b is  $0.34 \pm 0.06\text{‰}$  ( $n = 15$ ). Furthermore, the difference between SRM-915a and Atlantic sea water (collected off a peninsula in Santander Spain) is  $0.94 \pm 0.07\text{‰}$  ( $n = 5$ ), which is in agreement with the previously published value for Atlantic seawater of  $0.93 \pm 0.06\text{‰}$  (Tipper et al., 2010). There was a single measurement of SRM-3109a ( $0.42\text{‰}$ ;  $n = 1$ ); there are no currently published values with which to compare this value.

On the MIL Neptune Plus, the presence of Sr affected the measured Ca isotopic composition. In particular, Ca isotope measurements on the MIL Neptune Plus are sensitive to trace amounts of Sr, which appears to be ubiquitous in all Ca isotope and concentration standards (typical Sr concentration in Ca Specpure ICP standards, for example, is 0.05 ppb). A Sr sensitivity test was carried out where the production of doubly-charged species (i.e.,  $^{88}\text{Sr}^{++}$ ,  $^{86}\text{Sr}^{++}$ , and  $^{84}\text{Sr}^{++}$ ) was calibrated by monitoring the intensities of ion beams at masses 44, 43, and 42 produced by 1, 10, and 40 ppb Sr solutions in 0.5 N  $\text{HNO}_3$  (Table 2). Based on this calibration, we determined that, for example, a Sr concentration of 0.05 ppb in the sample will increase the measured ion beam at mass 44 by a sizeable 0.8 mV. As a result, all standards that were utilized in this study were purified using Eichrom's Sr Spec resin prior to use. All samples were plotted on a  $\delta^{44/42}\text{Ca}$ - $\delta^{43/42}\text{Ca}$  isotope-isotope plot, and characteristic deviations from the mass fractionation line was used to diagnose the presence of Sr (Fig. 2). There were no samples that were obviously influenced by Sr included in our dataset.

#### 2.4.3. Isotopic notation

The Ca isotope ratios of solid (*s*) and aqueous Ca (*f*) are reported using typical delta notation ( $\delta^{44/42}\text{Ca}$ ) relative to NIST SRM-915a:

$$\delta^{44/42}\text{Ca} = \left[ \frac{\left(\frac{^{44}\text{Ca}}{^{42}\text{Ca}}\right)_{\text{sample}}}{\left(\frac{^{44}\text{Ca}}{^{42}\text{Ca}}\right)_{\text{SRM915a}}} - 1 \right] \cdot 10^3 \quad (2)$$

The delta values reported herein represent the average of the replicates, and the error reported is twice the standard deviation (2SD) of the replicate analyses (typical values  $< 0.1\text{‰}$ ). In order to facilitate comparisons with previously

Table 1  
The  $\delta^{44/42}\text{Ca}$  of various standards measured at Penn State and compared to the literature.

Standard	$\delta^{44/42}\text{Ca}^a$ (‰)	n	Literature value <sup>a</sup> (‰)	Reference
SRM915b	$0.34 \pm 0.06$	15	$0.35 \pm 0.06$	Fantle and Tipper (2014)
Atlantic Sea Water <sup>b</sup>	$0.94 \pm 0.07$	5	$0.93 \pm 0.06$	Tipper et al. (2010)
SRM3109a	0.42	1	NA	NA

<sup>a</sup> All  $\delta^{44/42}\text{Ca}$  are reported relative to SRM915a, and the error is 2SD of n replicates.

<sup>b</sup> Collected on a beach off a peninsula in Santander, Spain.

Table 2

The intensities of the mass 44, 43, and 42 ion beams generated from  $^{88}\text{Sr}^{++}$ ,  $^{86}\text{Sr}^{++}$ , and  $^{84}\text{Sr}^{++}$  species, respectively. The intensities were measured from pure Sr solutions of 0 to 40 ppb.

[Sr] (ppb)	Intensity (mV)		
	Mass 44	Mass 43	Mass 42
0	4	<1	1
1	15	2	1
10	155	20	2
40	680	80	6

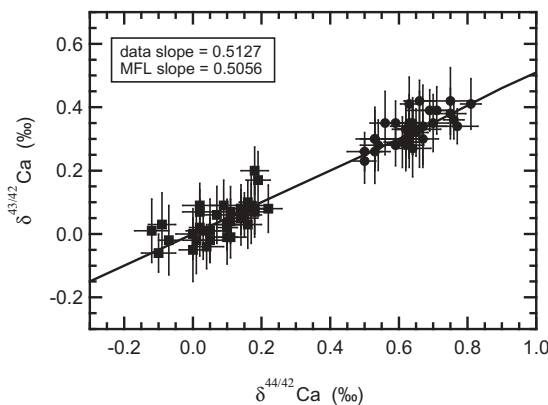


Fig. 2. Isotope-isotope ( $\delta^{43/42}\text{Ca}$  vs.  $\delta^{44/42}\text{Ca}$ ) plots of (a) gypsum (■) and solution (●) from laboratory experiments. All samples were measured with MC-ICP-MS at Penn State, using SRM-915a as the bracketing and normalizing standard.

published Ca isotope data, we report our isotope data in terms of  $^{44}\text{Ca}/^{40}\text{Ca}$  using the approximation below to convert measured  $^{44}\text{Ca}/^{42}\text{Ca}$  ratios to  $^{44}\text{Ca}/^{40}\text{Ca}$  ratios (Criss, 1999):

$$\delta^{44/40}\text{Ca} = \delta^{44/42}\text{Ca} \cdot \left( \frac{41.9586}{39.9626} \right) \cdot \left( \frac{39.9626 - 43.9555}{41.9586 - 43.9555} \right) \quad (3)$$

In this study, the Ca isotopic fractionation factor is reported as  $\Delta^{44/40}\text{Ca}_{s-f}$ :

$$\Delta^{44/40}\text{Ca}_{s-f} = \delta^{44/40}\text{Ca}_s - \delta^{44/40}\text{Ca}_f \quad (4)$$

The determination of fractionation factor is discussed in detail in Section 4.1.

#### 2.5. Calcium isotopic analysis by thermal ionization mass spectrometry (TIMS)

The Ca isotopic compositions of the Grotta Bella gypsum, drip water, limestone, and spring water were measured using a Finnigan Triton thermal ionization mass spectrom-

eter (TIMS) at GEOMAR in Kiel, Germany. The large gypsum needles were sonicated four times in water for 5 min to remove external impurities. All gypsum samples were then dissolved in 3 N HNO<sub>3</sub> at 90°C overnight. Limestone samples were powdered and dissolved in 2.2 N HCl, evaporated to dryness and then resuspended in 3 N HNO<sub>3</sub>. Water samples were acidified in the field and dried down at 90°C overnight and resuspended in 3 N HNO<sub>3</sub>. Following the dry down, each sample (~3 µg Ca) was equilibrated with a <sup>43</sup>Ca–<sup>48</sup>Ca double spike, purified using MCI Gel (Biorad), and loaded onto outgassed Re filaments with a TaCl<sub>5</sub> activator (Heuser et al., 2002). Measurements of an in-house CaF<sub>2</sub> standard ( $\delta^{44}\text{Ca}_{\text{SRM915a}} = 1.43 \pm 0.06\%$  2SD,  $n = 4$ ) were conducted in each barrel, while the variability of SRM-915a measured in all barrels was 0.15% 2SD ( $n = 15$ ). Procedural blanks were typically <0.5% of the total Ca processed.

The gypsum samples OP-1, OP-2, OP-3, and OP-4 were also measured by thermal ionization mass spectrometry (Finnigan Triton) at the University of California, Berkeley (Center for Isotope Geochemistry, CIG). The samples were selected from the same sample set collected in June 2009, but represent distinct and separate crystals that were sampled, dissolved, and chromatographically purified in June 2010 in Berkeley. Duplicate analyses of all samples were conducted, with the reported error representing twice the standard deviation of the duplicate analyses. Internal reproducibility at Berkeley is <0.05% on the Triton, while long-term measurements of the seawater yield a  $\delta^{44}\text{Ca}$  value of 1.89% on the SRM-915a scale (Fantle and Higgins, 2014).

### 3. RESULTS

#### 3.1. Microbial growth and solution chemistry

Experiment results are summarized in Tables 3 and 4. The experiments lasted for 50–53 days (Series 1) and 54–65 days (Series 2). In both series, cell density increased between Day 4 and Day 20, after which a slower growth phase was observed for the remainder of the incubations (Fig 3; Appendix B). Final cell densities ranged between  $7.1 \cdot 10^8$  and  $1.2 \cdot 10^9$  cells/ml regardless of the initial cell densities (i.e.,  $1 \cdot 10^5$ – $1 \cdot 10^8$  cells/ml). By the end of the experiments, the cells had produced between 11.3 and 24.5 ppm of carbohydrates in the biotic experiments, compared to 1.9–8.3 ppm of carbohydrates present in the abiotic controls. The dissolved organic carbon (DOC) content of the final culture media was 26.3–672 ppm in the biotic experiments, and 14.1–47.1 ppm in the abiotic controls. Total organic carbon (TOC) in the solid fraction was 0.80–3.05 wt% in biotic experiments and 0 wt% in the abiotic controls (Table 3).

The evolution of pH and SO<sub>4</sub><sup>2-</sup> concentration correlated with cell density in all biotic cultures (Fig. 3; Appendix A), as expected for a microorganism that oxidizes S<sup>0</sup> to sulfuric acid. The pH dropped from 4.2 (initial pH of the media) to between 1.6 and 1.3 during the fast growth phase, and stabilized at this value when cell growth rate slowed. Therefore, in all experiments, the pH was between 1.6 and 1.3

at the onset of gypsum precipitation. The increase in SO<sub>4</sub><sup>2-</sup> concentrations and decrease in pH in the killed and abiotic controls successfully mimicked the biotic experiments (Appendix B).

In each experiment, a measured drop in Ca<sup>2+</sup> concentration generally corresponded to the observed onset of gypsum precipitation (Table 4; Appendix B). Based on ICP-AES measurements of the digested final fluids from the experiments, the Ca<sup>2+</sup> concentration drop over the course of the experiments was ~7 to 16 mM in Series 1, and ~9 to 18 mM (initial [Ca<sup>2+</sup>] = 50 mM), or ~14 to 24 mM (initial [Ca<sup>2+</sup>] = 70 mM) in Series 2. The uncertainty in Ca<sup>2+</sup> concentrations in all experiments, calculated as 1 SD of the measurements of two independent aliquots of the final Series 2 solutions, was between 0.8 and 4.8 mM (Table B1). In both series, the drop in Ca<sup>2+</sup> concentration and the observed onset of gypsum precipitation occurred earlier in the controls than in the biotic experiments by approximately 20 days.

Gypsum saturation states, defined as the ion activity product over the solubility product, and Ca<sup>2+</sup>:SO<sub>4</sub><sup>2-</sup> ratios were calculated at each time point where both Ca<sup>2+</sup> and SO<sub>4</sub><sup>2-</sup> concentrations were measured. Maximum saturation states, which occurred just prior to the onset of precipitation, ranged between 1.5 and 3.2 (Series 1) and 1.0 and 1.5 (Series 2). The saturation state was higher in the biotic experiments relative to the controls by ~1.5 (Series 1) and ~0.4 (Series 2). The error in calculated saturation state was estimated to be <0.27 by error propagation of the standard deviation of duplicate Ca<sup>2+</sup> (1 SD = 4.8 mM) and SO<sub>4</sub><sup>2-</sup> (1 SD = 1.40 mM) concentration measurements. The Ca<sup>2+</sup>:SO<sub>4</sub><sup>2-</sup> ratio at the onset of gypsum precipitation in Series 1 was between 1.0 and 1.1 for the biotic experiments and 0.60 and 0.62 for the killed and abiotic controls. In Series 2, the Ca<sup>2+</sup>:SO<sub>4</sub><sup>2-</sup> ratio was 1.0 to 2.4 in the biotic experiments and 2.2–4.9 in the controls.

While generally in agreement with the Series 2 Ca<sup>2+</sup> concentration temporal trends, the concentration trends of the Series 1 experiments appear to be affected by systematic error (Figs. B1 and B2), such that some aliquots had higher Ca<sup>2+</sup> concentrations than the initial solution that could not be explained by instrumental error alone. As there is no secondary source of Ca<sup>2+</sup> in the experiments, and the measured aliquots were not initially digested in H<sub>2</sub>O<sub>2</sub>, we suggest that the concentration measurements were influenced by the presence of organics. As a result, we do not rely on the rate estimates from the Series 1 concentration data in the discussion that follows.

#### 3.2. Gypsum morphology and precipitation rates

All experiments yielded between 28 and 186 mg of gypsum per 75 mL of total solution (Table 4). Precipitates produced in the biotic experiments were shorter in length than the crystals from the abiotic control (Fig. 4), and occurred as single needles, clusters, and were either bladed and sheet-like or acicular. The abiotic control crystals only occurred as single long needles. The crystals in the biotic experiments consistently had smaller aspect ratios (defined as long/short dimension; AR =  $8.05 \pm 3.99$ ) as compared to the abiotic

Table 3  
Summary of experimental initial conditions and results.

Exp # <sup>a</sup>	[Ca] <sub>initial</sub> (mM)	Cell density		log R <sup>b</sup> (μmol/h)	Solution and crystal characterization						f <sub>Ca</sub> <sup>g</sup>		Ca isotopes		
		Initial (cells/ml)	Final (cells/ml)		Ω <sub>max</sub> <sup>c</sup>	pH <sub>ppt</sub> <sup>d</sup>	Tot. carb <sup>e</sup> (ppm)	DOC <sub>fluid</sub> (ppm)	TOC <sub>solid</sub> (wt%)	Aspect Ratio <sup>f</sup>	(1)	(2)	δ <sup>44</sup> Ca <sub>f</sub> <sup>h</sup>	δ <sup>44</sup> Ca <sub>s</sub> <sup>h</sup>	Δ <sup>44</sup> Ca <sub>s-f</sub> <sup>i</sup>
Media												1.07 ± 0.03			
<i>SERIES 1</i>															
1P-1	50	~1·10 <sup>5</sup>	7.7·10 <sup>8</sup>	0.52 ± 0.44	2.8	1.6	18.5	34.5	0.77	14.0 ± 3.21	0.139	0.154	1.32 ± 0.03	0.02 ± 0.03	-1.30 ± 0.04
2P-1	50	~1·10 <sup>6</sup>	7.8·10 <sup>8</sup>	0.34 ± 0.44	2.7	1.6	21.6	243	3.05	12.6 ± 1.63	0.0938	0.0436	1.13 ± 0.03	-0.19 ± 0.04	-1.32 ± 0.05
3P-1	50	~1·10 <sup>7</sup>	7.1·10 <sup>8</sup>	0.18 ± 0.87	3.2	1.6	24.5	26.3	1.37	9.30 ± 1.17	0.222	0.173	1.39 ± 0.03	0.06 ± 0.03	-1.32 ± 0.04
7 K-1	50	~1·10 <sup>8</sup>	1·10 <sup>8</sup>	0.19 ± 0.36	1.7	1.6	8.0	28.7	0	13.9 ± 1.49	0.175	0.133	1.32 ± 0.01	0.23 ± 0.02	-1.09 ± 0.02
8C-1	50	0	0	0.16 ± 0.57	1.5	1.6	1.7	34.2	0	39.2 ± 5.39	0.162	0.133	1.28 ± 0.05	0.31 ± 0.03	-0.97 ± 0.04
<i>SERIES 2</i>															
1P-2	50	~1·10 <sup>6</sup>	8.3·10 <sup>8</sup>	0.21 ± 0.54	1.3	1.4	20.5	385	0.81	5.58 ± 0.73	0.194	0.208	1.60 ± 0.09	0.19 ± 0.07	-1.41 ± 0.11
2P-2	50	~1·10 <sup>6</sup>	9.0·10 <sup>8</sup>	0.68 ± 0.35	1.4	1.5	18.1	672	2.15	6.41 ± 0.92	0.217	0.189	1.34 ± 0.03	0.25 ± 0.07	-1.09 ± 0.08
4C-2	50	0	0	-0.09 ± 0.65	1.1	1.5	8.3	14.1	0	33.7 ± 5.32	0.114	0.238	1.34 ± 0.02	0.34 ± 0.04	-1.01 ± 0.04
5P-2	70	~1·10 <sup>6</sup>	1.1·10 <sup>9</sup>	0.14 ± 0.32	1.4	1.3	13.9	97.1	0.44	4.28 ± 0.46	0.223	0.198	1.60 ± 0.02	0.34 ± 0.04	-1.26 ± 0.04
6P-2	70	~1·10 <sup>6</sup>	1.2·10 <sup>9</sup>	0.18 ± 0.32	1.5	1.4	11.3	584	0.80	4.18 ± 0.38	0.220	0.204	1.43 ± 0.03	0.13 ± 0.06	-1.30 ± 0.07
8C-2	70	0	0	0.37 ± 0.45	1.0	1.6	1.9	47.1	0	22.7 ± 1.66	0.163	0.0889	1.30 ± 0.06	0.42 ± 0.04	-0.88 ± 0.07

<sup>a</sup> Biotic precipitation experiments are denoted by P, sterile controls are denoted by C, and the killed control is denoted with K. The '-1' refers to series 1 experiments and '-2' refers to series 2 experiments. The initial δ<sup>44</sup>Ca of the media before inoculation is denoted as 'media' and is the average of the δ<sup>44</sup>Ca measurement of the media in Series 1 and 2 (error is 1SD of the two δ<sup>44</sup>Ca measurements).

<sup>b</sup> Error is the standard deviation of rates calculated from Monte Carlo generated concentration profiles, which were constrained by the error in the Ca concentration measurements. Rates are not surface area normalized due to difficulty in separating organic matter from crystals to obtain accurate BET surface area measurements.

<sup>c</sup> Highest measured gypsum saturation state (Ω = IAP/Ksp) throughout the experiment as calculated using PHREEQC (Ksp = 2.62·10<sup>5</sup>; T = 25 °C). The errors were propagated from the standard deviations between duplicate Ca and SO<sub>4</sub><sup>2-</sup> concentration measurements, and are <0.2.

<sup>d</sup> pH of solution at the time of gypsum precipitation. The series 1 pHs were measured using pH paper and therefore are less precise than the series 2 pHs, which were measured via pH probe. Initial pH in all experiments was 4.2.

<sup>e</sup> Total carbohydrate concentration measurements of the media at the termination of the experiments using phenol-sulfuric acid assay (Dubois et al., 1956).

<sup>f</sup> Longest dimension by the shortest dimension. Errors are standard error of the mean = stdev/√n.

<sup>g</sup> Mass fraction of total initial Ca in the precipitates calculated in 2 ways. (1) is determined via final gypsum yield per experiment (Table 4) and (2) is determined by Ca concentrations of the final fluid via ICP-AES.

<sup>h</sup> Error is 2SD of 3–4 replicates. See Appendix A for raw data.

<sup>i</sup> Calculated using Eq. (4). Error = √((SD<sub>δ44Cas</sub>)<sup>2</sup> + (SD<sub>δ44Caf</sub>)<sup>2</sup>).

Table 4  
Duration of gypsum precipitation experiments and crystal yields.

Exp#	Gypsum yield (mg)	Onset of precipitation (day)	Time of termination (day)	Time crystals remained in solution (days)
<i>SERIES 1</i>				
1P-1	99	45	51	6
2P-1	28	45	53	8
3P-1	111	45	51	6
7 K-1	86	22	52	30
8C-1	86	22	52	30
<i>SERIES 2</i>				
1P-2	135	54	63	9
2P-2	122	57	65	8
4C-2	154	36	54	18
5P-2	180	36	62	26
6P-2	186	44	61	17
8C-2	81	28	54	26

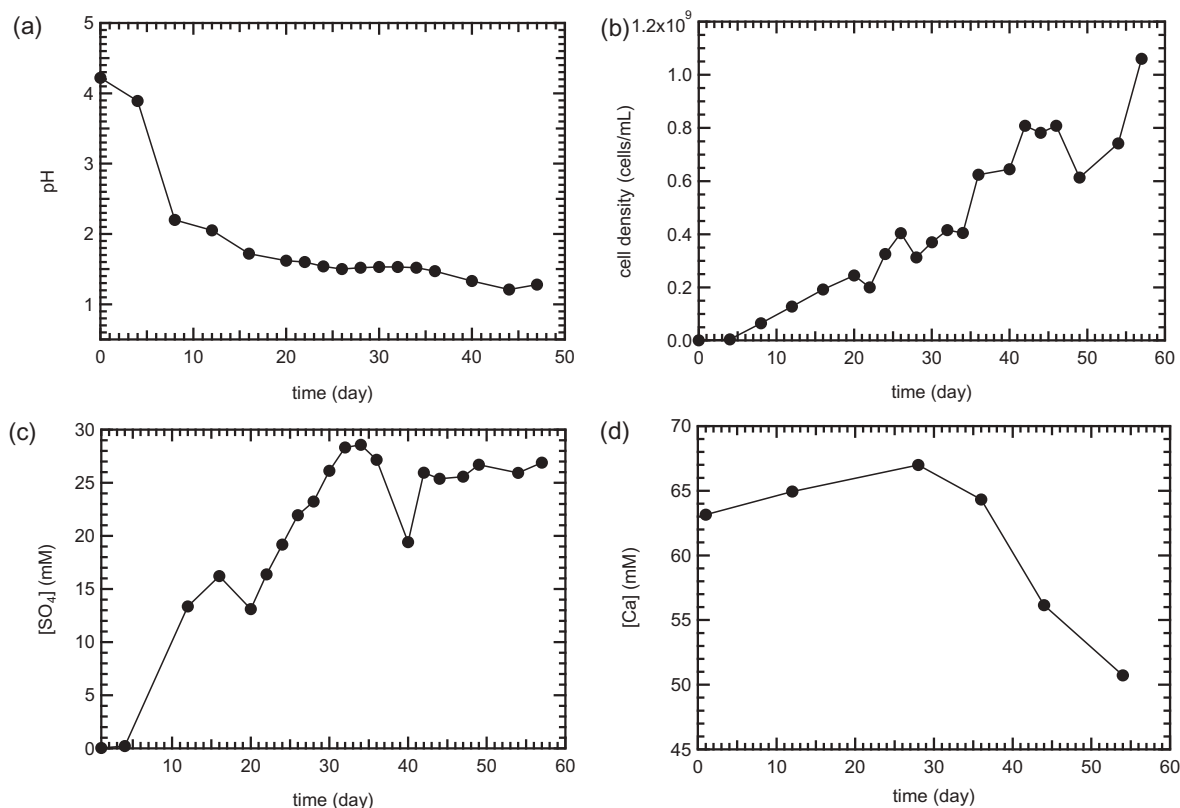


Fig. 3. Representative example of the temporal evolution of cultures (biotic experiment 5P-2), indicating evolution of (a) pH, (b) cell density, (c) sulfate concentration and (d) calcium concentration over experimental time scales.

controls ( $AR = 31.9 \pm 8.40$ ; Table 3). The killed control produced crystals that were intermediate with respect to aspect ratios ( $AR = 13.9 \pm 1.49$ ) and morphological diversity, relative to the biotic and abiotic experiments. Microbial gypsum precipitation rates ( $\log R$ ) ranged between  $0.14 \pm 0.32$  and  $0.68 \pm 0.25$   $\mu\text{mol/h}$ , whereas gypsum precipitation rates in the abiotic controls were  $-0.09 \pm 0.46$  to  $0.37 \pm 0.45$   $\mu\text{mol/h}$ .

### 3.3. Experiments: Ca isotopic composition ( $\delta^{44}\text{Ca}$ )

All experimental gypsum precipitates were isotopically lighter than the initial solution. In all experiments, the initial  $\delta^{44}\text{Ca}$  of  $\text{Ca}^{2+}(\text{aq})$  in the media was  $1.07\text{‰}$ , as the Ca source in Series 1 ( $\delta^{44}\text{Ca} = 1.09\text{‰}$ ) and Series 2 ( $\delta^{44}\text{Ca} = 1.05\text{‰}$ ) was the same; the reported measurements are considered replicates and were averaged. The isotopic

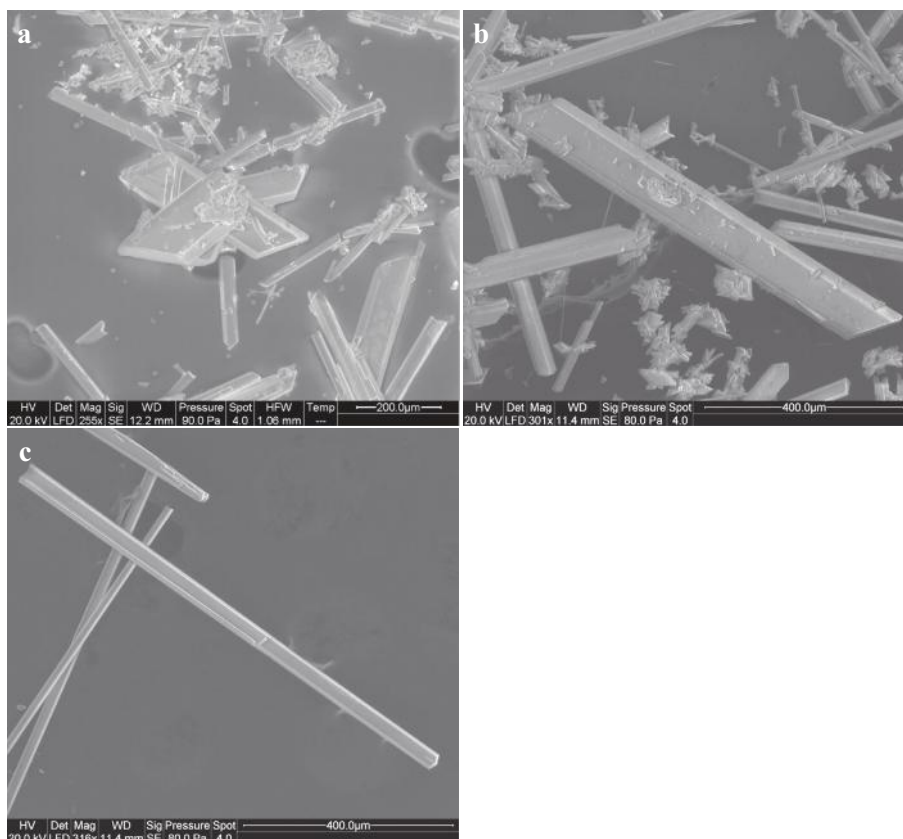


Fig. 4. Scanning electron micrographs of laboratory-precipitated gypsum from (a) biotic experiment 1P-2, (b) killed control 7K-1, and (c) abiotic control 8C-1.

composition of all precipitates ( $\delta^{44}\text{Ca}_s$ ) ranged between  $-0.19 \pm 0.04\text{‰}$  and  $0.42 \pm 0.04\text{‰}$ , while the isotopic composition of the final solutions ( $\delta^{44}\text{Ca}_f$ ) ranged between  $1.13 \pm 0.03\text{‰}$  and  $1.60 \pm 0.09\text{‰}$ . The biotic experiments produced precipitates with  $\Delta^{44}\text{Ca}_{s-f}$  values that were on average  $-1.29 \pm 0.10\text{‰}$  (relative to the final solution), while precipitates from the abiotic controls had  $\Delta^{44}\text{Ca}_{s-f}$  values that were  $-0.95 \pm 0.07\text{‰}$ . The microbially mediated gypsum precipitates had  $\delta^{44}\text{Ca}$  values that were, on average,  $0.3\text{‰}$  lower than the abiotic controls (Fig. 5). In comparison, precipitates from the killed control had a  $\Delta^{44}\text{Ca}_{s-f}$  value of  $-1.09\text{‰}$ , or  $-0.14\text{‰}$  lower than the average  $\delta^{44}\text{Ca}$  of the abiotic controls.

### 3.4. Frasassi cave system: Ca isotopic composition ( $\delta^{44}\text{Ca}$ )

The gypsum crystals collected from Grotta Bella (GB) ranged from micro-crystalline ( $\text{AR} = 2.03 \pm 1.04$ ) to wall crust ( $\text{AR} = 4.42 \pm 1.10$ ), and small ( $\text{AR} = 7.20 \pm 4.50$ ) and large needles ( $\text{AR} = 11.6 \pm 5.19$ ). The  $\delta^{44}\text{Ca}$  range observed in the gypsum crystals from GB is approximately  $0.8\text{‰}$  (Table 5; Fig. 6). There is a coherent trend in the  $\delta^{44}\text{Ca}$  values relative to aspect ratio, such that as aspect ratio increases, the  $\delta^{44}\text{Ca}$  decreases by  $\sim 0.8\text{‰}$  ( $\delta^{44}\text{Ca}_{\text{GB\_microcrystals}} = 1.15 \pm 0.06\text{‰}$ ;  $\delta^{44}\text{Ca}_{\text{GB\_needles}} = 0.44 \pm 0.13\text{‰}$ ).

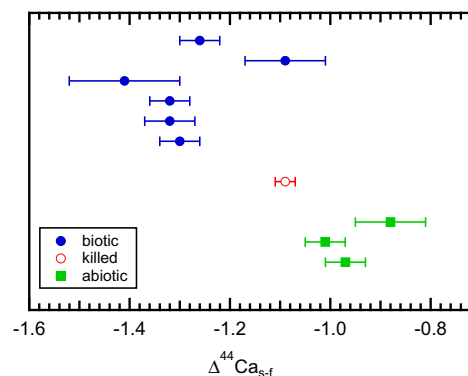


Fig. 5. The Ca isotopic fractionation factor ( $\Delta^{44}\text{Ca}_{s-f}$ ) of biotic experiments, killed control, and abiotic controls.

## 4. DISCUSSION

### 4.1. Calcium isotopic fractionation associated with gypsum precipitation in the presence of microbes

A major objective of this study was to determine whether or not microbes influence the Ca isotopic composition of minerals, in order to evaluate the impact of microbial life on interpretations of Ca isotopes in natural systems and the rock record. In our experiments, the

Table 5

The Ca isotopic composition of natural samples collected from the Frasassi cave system and the surrounding area measured by TIMS at GEOMAR in Keil and at the CIG in Berkeley.

Sample #	Type	Aspect Ratio <sup>a</sup>	Temp <sup>b</sup> °C	pH <sup>c</sup>	Conductivity <sup>c</sup> μS/cm	δ <sup>44</sup> Ca ‰, SRM-915a	2SD <sup>d</sup> ‰	Location
	<i>Limestone</i>							
FG-3B	Cave limestone, sampled from inside cave					1.30	0.09	San Vittore
FG-10	Massiccio limestone, road outcrop					1.04	0.05	Gola di Frasassi
	<i>Grotta Bella Gypsum</i>							
OP-1	Microcrystalline gypsum (GEOMAR)	2.03 ± 1.04	13	0		1.17	0.06	Grotta Bella
	Microcrystalline gypsum (Berkeley CIG)					1.13	0.01	
OP-2	Small needle gypsum (GEOMAR)	7.20 ± 4.50	13	0		0.69	0.11	Grotta Bella
	Small needle gypsum (Berkeley CIG)					0.78	0.04	
OP-3	Wall crust gypsum (GEOMAR)	4.42 ± 1.10	13	0		0.97	0.20	Grotta Bella
	Wall crust gypsum (Berkeley CIG)					0.94	0.03	
OP-4	Large needle gypsum (GEOMAR)	11.6 ± 5.19	13	0		0.46	0.13	Grotta Bella
	Large needle gypsum (Berkeley CIG)					0.43	0.06	
	<i>Local waters</i>							
FG-1	Fissure spring water (sulfidic)		20.3	7.2	3030	1.22	0.05	San Vittore
FG-3	Cave spring water (sulfidic)		21.0	7.3	1700	1.07	0.20	San Vittore
FG-5	Cave spring 2 water (sulfidic)		20.5	7.3	1682	1.03	0.08	San Vittore
FG-7	Sentino River water sample, upstream of seeps		19.2	7.8	830	0.86	0.10	San Vittore
GV-1	Gorgo Vivo spring (sulfide-free)		19.4	7.3	550	0.97	0.07	Serra San Quirico
DW-249	Drip water					1.13	0.05	Grotta Bella
	<i>Sea water</i>							
SWB-1	Mediterranean Seawater <sup>e</sup>					1.82	0.01	Bejaia, Algeria

<sup>a</sup> Long dimension by short dimension. Error is the standard deviation of aspect ratios of multiple crystals in a sample.

<sup>b</sup> Temperature of solid samples is ambient temperature in the caves where the solids precipitated.

<sup>c</sup> pH probe standardized in the field with pH 7 and pH 10 buffers (measured values of pH 4, 7, and 10 buffers after sample measurement were 4.04 ± 0.01, 7.04 ± 0.01, and 9.99 ± 0.01, respectively. A 1000 μS/cm conductivity standard was measured in the field (=1023 μS/cm). The pH of solid samples were measured with pH paper.

<sup>d</sup> External reproducibility is two times the standard deviation (2SD) of 2 to 4 replicate analyses.

<sup>e</sup> Collected on the shore of a beach and measured with MC-ICPMS at Penn State ( $n = 4$ ). The measured <sup>44</sup>Ca/<sup>42</sup>Ca ratio was converted to <sup>44</sup>Ca/<sup>40</sup>Ca (Eq. (3)). The δ<sup>44</sup>Ca is lighter than previously measured Mediterranean sea water (Tipper et al., 2006), which is likely consequence of mixing with terrestrial waters.

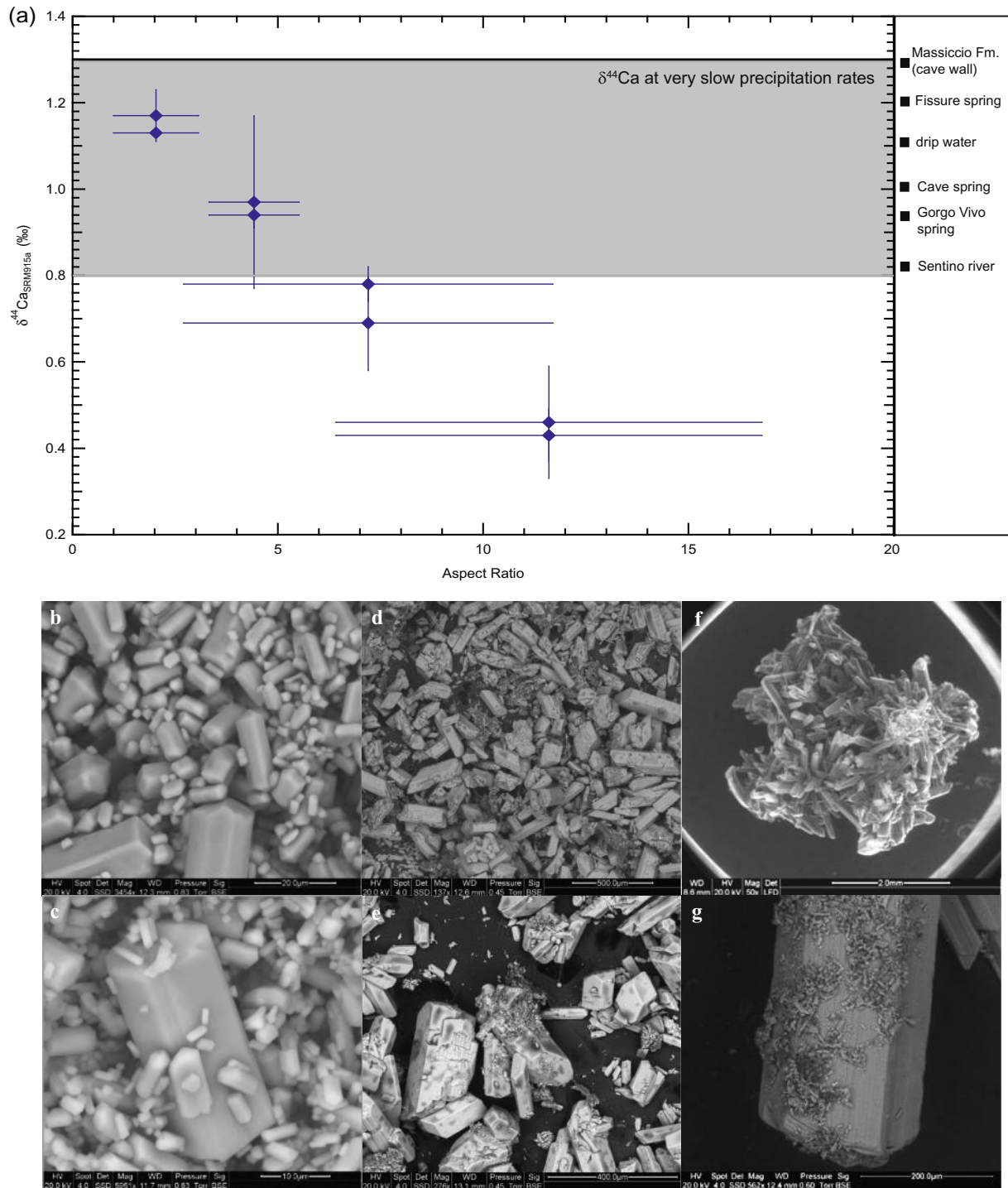


Fig. 6. (a) Calcium isotopic composition ( $\delta^{44}\text{Ca}$ ) of gypsum from Grotta Bella in the Frasassi cave system (Italy). The source Ca is assumed to be the limestone wall (solid black line). The  $\delta^{44}\text{Ca}$  of the drip water collected from Grotta Bella, as well as other waters such as the Fissure spring ( $\delta^{44}\text{Ca} = 1.22\text{‰}$ ), Gorgo Vivo spring ( $\delta^{44}\text{Ca} = 0.97\text{‰}$ ) and Sentino River ( $\delta^{44}\text{Ca} = 0.86\text{‰}$ ), are indicated. The gray area denotes the isotopic composition assumed for crystals that precipitate close to chemical equilibrium (i.e., at very slow rates) without considering isotopic distillation. The SEM images are of the (b and e) microcrystalline, (c and f) wall crust and (d and g) needle gypsum morphologies found in the caves. Analyses of completely separate samples by TIMS at GEOMAR in Kiel, Germany and the University of California, Berkeley (Center for Isotope Geochemistry, CIG) are shown.

presence of a microbial isotope effect was confirmed by comparing the fractionation factors associated with gypsum precipitation in biotic cultures and abiotic controls.

The fractionation factors were constrained using a Rayleigh distillation model, assuming that the measured fluid  $\delta^{44}\text{Ca}$  values represent well-mixed solutions (as outlined in

Harouaka et al., 2014; Figs. D1 and D2). The resultant average fractionation factor ( $\alpha_{s-f}$ ) associated with the biotic experiments is  $0.9989 \pm 0.0002$ , while that associated with the abiotic controls is  $0.9991 \pm 0.0001$  (Table A4, Fig. D3). Therefore, the experimental biological isotope effect is  $-0.3\text{‰}$ . From a broad perspective, the calculated  $\alpha_{s-f}$  values are consistently less than one, which is in agreement with Ca isotope fractionation observed in previous abiotic gypsum precipitation experiments (Harouaka et al., 2014; Blattler and Higgins, 2014), as well as in  $\text{CaCO}_3$  precipitation experiments (Gussone et al., 2003, 2005, 2007; Lemarchand et al., 2004; Tang et al., 2008, 2011; Gussone et al., 2011; Reynard et al., 2011). The biological isotopic fractionation effect ( $-0.3\text{‰}$ ) is significant given that typical isotopic variability in the rock record is on the order of tenths of a permil (e.g., Payne et al., 2010; Hinojosa et al., 2012; Jost et al., 2014; Kasemann et al., 2014; Griffith et al., 2015; DuVivier et al., 2015).

Before exploring the mechanisms and potential utility of the biological isotope effect, we note that a few of the experimental precipitates (Expts. 1P-2, 5P-2 and 8C-2) were not well fit by the Rayleigh model (Fig. D2). This suggests either that the precipitates are isotopically heterogeneous or that the measured  $f_{Ca}$  values are inaccurate. Isotopic heterogeneity has been hypothesized to exist in previous experimental work, in which the  $\delta^{44}\text{Ca}$  of calcite precipitated within *Desulfobulbus mediterraneus* biofilm was  $0.5\text{‰}$  heavier than the calcite precipitated from solution (Krause et al., 2012). It is possible that similar isotopic heterogeneity existed in the gypsum crystals that precipitated within the *A. thiooxidans* biofilm, compared to precipitates formed from solution and on  $\text{S}^0$  granules. Because we did not homogenize the solids prior to sub-sampling the precipitates, the extent of isotopic heterogeneity in the solid is unknown.

A mass balance-based calculation of the solid  $\delta^{44}\text{Ca}$  suggests the possibility of a heterogeneous solid in a few experiments, assuming accurate  $f_{Ca}$  values (Table A4). However, resampling and reanalysis of precipitates from biotic experiment 1P-2 and abiotic control 8C-2 indicates that at the scale at which the precipitates are sampled, heterogeneity is not strongly expressed (Table A3). Additionally, precipitation of gypsum that is as much as  $-1\text{‰}$  offset from the measured value (difference between measured  $\delta^{44}\text{Ca}_s$  and mass balance derived  $\delta^{44}\text{Ca}_s$  is  $\approx 1\text{‰}$ ; Table A4) requires a fractionation factor associated with precipitation that is quite low ( $\alpha_{s-f} \sim 0.9976$  or  $\Delta^{44}\text{Ca}_{s-f} \sim -2.4\text{‰}$ ). This is well outside of the range of  $\alpha_{s-f}$  values observed in previous gypsum and  $\text{CaCO}_3$  experiments, especially at the low precipitation rates observed in our experiments (Fantle and DePaolo, 2007; Tang et al., 2008; DePaolo, 2011; Nielsen et al., 2012; Harouaka et al., 2014).

Instead, inaccuracies in  $f_{Ca}$  best explain the discrepancy between the measured and calculated  $\delta^{44}\text{Ca}$  of the solid. The  $f_{Ca}$  values reported herein were calculated in three ways: using (1) aqueous Ca concentrations (ICP-AES), (2) measurements of the mass of gypsum removed, and (3) an isotopic mass balance approach (Table A4). Constraints on  $f_{Ca}$  based on the former two methods suffer from systematic errors, such that the values obtained likely represent

minimum estimates (Table A4). The error is likely to have been caused by mass loss during sample dry down and during weighing due to static repulsion, and/or during filtration. Given these systematic errors, the accuracy and precision of the Ca isotope analyses, and the difficulty generating and sampling extensive isotopic heterogeneity, we consider the mass balance derived  $f_{Ca}$  to be robust. This conclusion requires the assumption of an isotopically homogenous solid at the scale of sampling.

Finally, given our analysis of the fractionation factor associated with microbially mediated gypsum precipitation, we consider the  $-0.3\text{‰}$  biological isotope effect to be a robust result. It is worth noting, however, that there is not complete agreement between the  $\alpha_{s-f}$  determined for the abiotic controls and  $\alpha_{s-f}$  determined in previous unstirred abiotic gypsum precipitation experiments at similar saturation states (Harouaka et al., 2014). There are sufficient differences in the experimental set up and solution composition between the two studies (i.e., solution chemistry, temperature, and the presence of additional nucleation sites provided by the  $\text{S}^0$  granules) that may affect both the morphology (e.g., Edinger, 1973; Cody, 1991; Bosbach and Hochella, 1995; Hamdona and Hadad, 2007) and  $\alpha_{s-f}$  of the gypsum precipitates (Harouaka et al., 2014). Thus, while we cannot conclusively explain the disparity between the abiotic control and previous abiotic work, we can explain the microbial influence on the  $\alpha_{s-f}$  of gypsum precipitation under the conditions imposed in this study.

## 4.2. Mechanism of Ca isotopic fractionation in microbially mediated gypsum

### 4.2.1. Microbial inhibition of gypsum precipitation

Previous investigations of Ca isotopic fractionation during mineral precipitation suggest that fractionation factors are influenced by precipitation kinetics (Lemarchand et al., 2004; Tang et al., 2008, 2011), the identity of the precipitated phase (Gussone et al., 2005, 2011; Nielsen et al., 2012; Gonzales and Fantle, 2014), and the morphology of the resultant crystal (Harouaka et al., 2014). Precipitation kinetics and crystal morphology are generally governed by the nature of the crystal surface, namely surface energies and the rate of ion attachment and detachment, while mineral phase is a complex function of saturation state, kinetics, and temperature. We rule out bulk precipitation kinetics as a dominant control on isotopic fractionation in our biotic experiments because the biotic and abiotic controls precipitated at the same rate. We also dismiss mineral phase related isotope effects, because gypsum was the sole phase precipitated in our experiments, as confirmed by XRD analysis (Fig. B4), SEM images (Fig. 4) and EDS analyses. In addition, all other potential phases (e.g., calcite and hydroxyapatite) were substantially under saturated in our experiments.

Instead, we propose that a mineral surface control on Ca isotopic fractionation is likely given that the most distinct difference between gypsum precipitated in the abiotic controls and biotic experiments was in the aspect ratio of the precipitates (Fig. 7). While the biotic and control

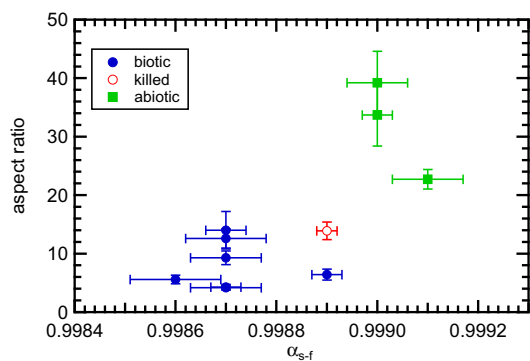


Fig. 7. Correlation between crystal aspect ratio and the measured isotopic fractionation factor ( $\alpha_{s-f}$ ) in the biotic experiments (●), killed control (○), and sterile controls (■).

experiments had comparable aqueous chemistries, the precipitates from the biotic experiments were significantly smaller than those of the controls (Fig. 4 and Table 3). Actively metabolizing microbes are known to produce extracellular organic compounds (e.g., Jones and Starkey, 1961; Riding and Awramik, 2000; Sutherland, 2001), and these compounds have been shown to influence gypsum morphology via growth inhibition (e.g., Barcelona and Atwood, 1978; Cody and Cody, 1989; Hamdona and Hadad, 2008). Biofilms, as well as living and dead cells, could also alter the morphology of gypsum by providing a template for gypsum nucleation and growth (e.g., Shultze-Lam et al., 1996; Rouchy and Monty, 2000; Vogel et al., 2009). Therefore, the observed differences in crystal aspect ratio between the two sets of experiments must be a consequence of the presence of living and, to a lesser extent, dead microbes.

Surface specific growth inhibition associated with the adsorption of organic molecules onto crystal surfaces can explain the experimental variability in crystal morphology and, hence, the Ca isotope data. Previous experimental studies of gypsum precipitation in the presence of organic molecules (e.g., Barcelona and Atwood, 1978; Cody and Cody, 1989; Hamdona and Hadad, 2008) have shown that growth on specific crystal faces is inhibited by the adsorption of organic molecules, which is consequently reflected in crystal aspect ratio. Growth inhibition, in particular via soluble organic molecules, is thought to occur when deprotonated carboxylic groups bind to surface Ca atoms (e.g., Barcelona and Atwood, 1978; Cody and Cody, 1991; Wang and Lee, 1993; DeOliveira and Laursen, 1997; Hazen et al., 2011). Accordingly, the most effective dissolved organic inhibitors in our experiments would be those with  $pK_{a1}$  values of  $\sim 2$ , because they will have deprotonated carboxylate groups at the low pH ( $< 2$ ) of the experimental solutions. The most common simple organic molecules with  $pK_{a1}$  values between 1 and 3 are amino acids (e.g., McMurry, 2004). We expect that our biotic experiments contain amino acids and polypeptides in solution, given that *A. thiooxidans* grown on  $S^0$  produces these organic compounds (Jones and Starkey, 1961). Insoluble organic molecules can also influence crystal growth, and

hence isotopic composition. Previous gypsum precipitation experiments demonstrated that C16:0 fatty acids (e.g., palmitic acid) and C18:0 fatty acids (e.g., stearic acid), in particular, sorb strongly onto gypsum surfaces (Barcelona and Atwood, 1978). Douglas and Mann (1994) demonstrated that insoluble organic substrates (such as C18:0 lipids) influence gypsum nucleation and crystallographic orientation during gypsum precipitation.

The observations regarding the interactions between organic molecules and gypsum are especially relevant to our experiments, given that biofilm produced by *Acidithiobacillus ferrooxidans* (a close relative of *A. thiooxidans*) is comprised dominantly of C16:0 and C18:0 lipids (54 wt%), C16:0 and C18:0 free fatty acids (8 wt%), and glucose (41 wt%), when grown on  $S^0$  in an acidic medium (Gehrke et al., 2008). Therefore, biofilm produced in our experiments could have affected the morphology, and thus the Ca isotopic composition, of the experimental precipitates via preferential sorption onto gypsum surfaces. Such a hypothesis is supported by observations in the biotic experiments of physical obstruction of growing step sites by biofilm (Fig. 8a). In addition, the killed control produced crystals that were slightly less fractionated ( $\sim 0.14\%$ ) than the biotic experiments. This suggests that cellular material, such as cell walls, may also inhibit gypsum growth, thereby impacting the Ca isotopic composition of gypsum. We therefore conclude that the observed 0.3‰ isotope effect can be explained by a combination of both soluble organic molecules and insoluble organic matter (i.e., biofilm, and living and dead cells) interacting with the growing crystal surface.

Calcium isotopic effects related to organic matter inhibition of growing crystals are likely to be more significant in solutions of a higher pH than in our experiments. As most soluble organic molecules are protonated in acidic solutions (e.g., McMurry, 2004), the isotope effect we observed (0.3‰) may reflect the influence of a relatively small fraction of the organic molecules available to bind to crystal surfaces at the low pH of the experiments. It is possible that a larger Ca isotopic effect may occur in solutions in which a greater proportion of organic molecules exist in the deprotonated form. For example, thermodynamic calculations using the geochemical modeling package PHREEQC (2.17.4466; Pitzer database; Parkhurst et al., 1999) indicate that the amino acid histidine, which behaves as a base in solution, is fully protonated at pH 1.6. The amount of protonated histidine drops to 61% at pH 5.6, while at pH 9, virtually no protonated histidine exists in solution. Given that biogenic calcite grows at  $pH > 8$ , which is much greater than the  $pK_{a1}$  of most common organic molecules, and is the dominant mineral forming in the modern ocean ( $pH \sim 8.1$ ), we speculate that similar organic-mineral interactions could also influence the Ca isotopic composition of marine calcite.

#### 4.2.2. Effect of biofilm formation on Ca isotopic fractionation

*Acidithiobacillus* biofilms formed during our experiments are known to sequester Ca from solution (e.g., Sutherland, 2001; Braissant et al., 2007; Uroz et al., 2009). If Ca is isotopically fractionated during its transfer

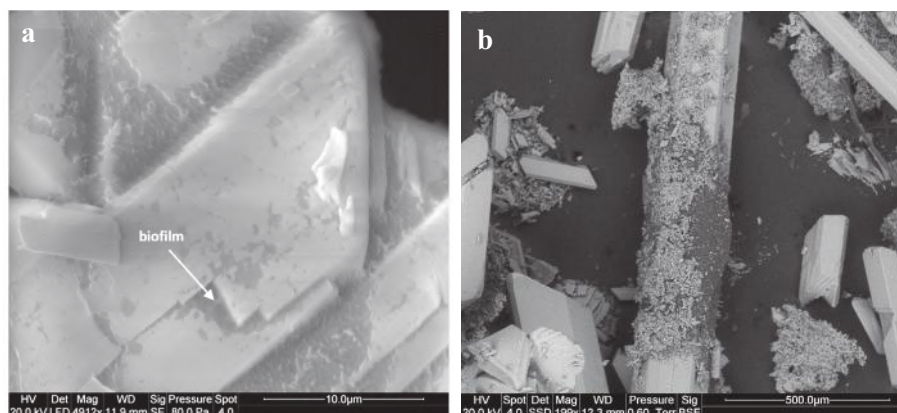


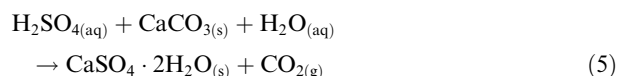
Fig. 8. Scanning electron microscope images of (a) the physical obstruction of growth sites on the gypsum surface by biofilm (Expt. IP-1) and (b) a gypsum needle collected from Grotta Bella coated by biofilm. The presence of biofilm is deduced by a high C peak on the EDS spectrograph. The intensity of the peak is maximum when the EDS is collected on the biofilm, and is present regardless of whether C or Cu tape was used.

into biofilm, then the mass balance used to determine  $f_{Ca}$  (Section 4.1) is missing a key component. This component can be roughly constrained by estimating the mass of biofilm produced in each experiment. Using the total organic carbon content (TOC; Table 3), and assuming that  $\sim 50\%$  of the biofilm is composed of glucose (FW 180.3 g/mol) and  $\sim 50\%$  of stearic acid (FW 284.4 g/mol; Gehrke et al., 2008), we estimate up to 1–10 mg of biofilm was produced in a given biotic experiment. Previous work suggests that biofilm binds  $\sim 0.15$  g Ca per gram of biofilm (Braissant et al., 2007), which translates to  $\sim 0.15$  to 1.5 mg of Ca sequestered in the biofilm in the biotic experiments. This mass represents less than  $\sim 1\%$  of either the mass of Ca precipitated in gypsum or the mass of the aqueous  $Ca^{2+}$  pool. In order for biofilm-bound Ca to affect the Ca isotope fractionation we observed in the crystals, the biofilm-bound fraction would have to have exceedingly high  $\delta^{44}Ca$  values (50–100‰). Given the extreme fractionation required, we conclude that such a scenario is unlikely.

In summary, assuming that the morphology of the crystal expresses the differences in growth rates of individual crystal faces, we propose that surface specific organic inhibition of mineral surfaces controlled the Ca isotopic fractionation associated with gypsum precipitation observed in our experiments. The remaining question is to what extent similar signals might be present in natural systems, and if Ca isotopes might be a useful component of a multi-proxy toolbox aimed at identifying the presence of life in the rock record.

#### 4.3. Calcium isotopic fractionation of Frasassi cave gypsum

The experiments in this study provide an interesting perspective on the Ca isotope compositions of gypsum collected from the Frasassi cave system. In the cave system, gypsum precipitates due to sulfuric acid dissolution of the limestone walls, according to the overall reaction:



and a  $\log R < -0.6$   $\mu\text{mol}$  gypsum/h (where  $R$  is the assumed gypsum precipitation rate; Jones, 2013). We assume that the limestone dissolution is rate-limiting, and that gypsum saturation is subsequently approached by the relatively rapid addition of  $SO_4^{2-}$  to solution, as was the case in our experiments. Previous experimental evidence and modeling suggests that the abiotic fractionation factor associated with gypsum precipitation at very slow precipitation rates is  $< 0.9995$  ( $< -0.5\%$ ; Harouaka et al., 2014). Therefore, we expect the fractionation factor of gypsum precipitation in the cave system to be in this range.

Unexpectedly, we found considerable variability in the Ca isotopic composition of the Frasassi cave gypsum. Overall, the  $\delta^{44}Ca$  of cave gypsum, relative to the limestone wall, correlates with the morphology of the gypsum crystals, such that the  $\delta^{44}Ca$  of low aspect ratio microcrystalline gypsum is similar to that of the limestone wall and gypsum  $\delta^{44}Ca$  decreases with increasing aspect ratio (Fig 6). Remarkably, large needles from Grotta Bella have  $\delta^{44}Ca$  values that are as much as 0.8‰ lower than the limestone cave wall (the assumed Ca source) based on measurements of different needles from the same collection conducted at GEOMAR and Berkeley (Table 5; Fig 6).

Though the cave wall likely doesn't reflect the solution from which gypsum precipitates, which is difficult to measure due to sampling limitations inherent to the cave system, it is a logical reference point. Given that the precipitation rate is likely to be slow (see below), and assuming that precipitation occurs at steady state, then the solution isotopic composition ( $\delta^{44}Ca_p$ ) is equal to ( $\delta^{44}Ca_s - \Delta^{44}Ca_{s-p}$ ), where  $\delta^{44}Ca_s$  is the isotopic composition of the cave wall and  $\Delta^{44}Ca_{s-p}$  is the fractionation factor associated with precipitation. Accordingly, if the fractionation factor is  $-0.5\%$  to  $0\%$ , then the fluid will be  $+0.5\%$  to  $0\%$  at steady state, and gypsum precipitated at steady state will have an isotopic composition similar to that of the cave wall. Thus, the  $\delta^{44}Ca$  of the microcrystalline gypsum is consistent with steady state precipitation. While it is also possible that the microcrystalline gypsum forms under non-steady conditions, this would require isotopic reequilibration with ambient solution (a process suggested

previously to have occurred over week time scales in abiotic gypsum experiments; Harouaka et al., 2014).

By contrast, the isotopic composition of the large needles is outside of the  $\delta^{44}\text{Ca}$  range expected for steady state precipitation. This leads to the hypothesis that the large needles precipitate out of steady state and fractionate to a greater extent than would be predicted at slow rates under non-steady state conditions. We suggest that both characteristics are consistent with a biological influence on mineral precipitation. Given that the needles are associated with microbial biofilms in Grotta Bella, we propose that the low  $\delta^{44}\text{Ca}$  values reflect isotopic fractionation caused by surface selective inhibition by organic molecules produced by active microbial communities (i.e., the same process inferred to fractionate Ca in the lab culturing experiments presented in this study).

There is no indication that the isotopically light needles form from an isotopically light Ca source, as all the measured seeps, drips, springs, and rivers have  $\delta^{44}\text{Ca}$  values that are considerably higher than the needles (Fig 6a; Table 5). There is no evidence that stream water contributes  $\text{SO}_4^{2-}$  to the cave wall gypsum, and therefore it is also unlikely that stream water  $\text{Ca}^{2+}$  is contributed to cave wall gypsum. The  $\delta^{34}\text{S}$  (relative to CDT) of the cave gypsum ( $\delta^{34}\text{S}_{\text{cave gypsum}} \approx -23\text{‰}$  to  $-16\text{‰}$ ) is lower than the cave air  $\text{H}_2\text{S}_{(\text{g})}$  by  $-12\text{‰}$  to  $-6\text{‰}$  (Galdenzi and Maruoka, 2003; Harouaka et al., 2013). This indicates that the gypsum did not form from stream  $\text{SO}_4^{2-}$  ( $\delta^{34}\text{S}_{\text{stream}} \approx +20$  to  $+22\text{‰}$ ), but rather from  $\text{SO}_4^{2-}$  supplied from the microbial oxidation of  $\text{H}_2\text{S}_{(\text{g})}$  in the cave atmosphere (Galdenzi and Maruoka, 2003). Thus, the primary source of  $\text{Ca}^{2+}$  to the cave gypsum is the corroding limestone. Further, while it is feasible that the  $\delta^{44}\text{Ca}$  range measured in the cave gypsum reflects variability in the host limestone (see Fantle and Tipper, 2014 for compilation of limestone data over geologic time), it is not likely that such variability occurs in the cave walls over the small spatial scales that characterize an individual cave room. Therefore the variation in the  $\delta^{44}\text{Ca}$  observed in the Grotta Bella gypsum must be related to the local chemistry and microbiology of the thin film of solution on the cave wall from which the gypsum precipitates.

Multiple arguments can be made against a rate-dependent kinetic isotope effect in the cave needles, including a simple box model of the Grotta Bella system (Appendix E). The simplest argument, however, is this: in order for the needles to fractionate on the order of  $-1\text{‰}$  according to the sort of rate effects seen previously, they would have to precipitate at a rate  $>400 \mu\text{mol}/\text{m}^2/\text{h}$  (e.g., Tang et al., 2008; Harouaka et al., 2014). This rate is more than fifteen times faster than the maximum estimated rate of gypsum precipitation in Frasassi ( $R < 26.3 \mu\text{mol}/\text{m}^2/\text{h}$ ; Jones, 2013). The estimated gypsum precipitation rate was determined from the dissolution of calcite tablets exposed to the cave atmosphere over a period of two to five years, and normalized to the surface area of the tablet. Therefore the field based rate is most likely an overestimate, given that the microcrystalline gypsum that precipitated on the tablets has considerably more surface area than the tablet itself. The resulting surface area normalized rate must then be lower than the estimate above.

Ultimately, the data presented here suggest two manners in which the Ca isotopic composition of a mineral such as gypsum might be used to identify the presence of biology. One approach is the measurement of populations of microcrystalline precipitates, with the recognition that significant post-formational exchange can (and likely does) occur. In order for this approach to yield useful results, it is necessary to sample a large proportion of the microcrystalline population and document the isotopic variability in that population. The assumption of the technique is that all precipitates grew under similar conditions (saturation state, rate, pH, etc), but are variably impacted by post-formational exchange. Accordingly, the aim of this approach is to attempt to look through the complication of exchange, to find the tail of the distribution. If this tail has an isotopic composition that cannot be explained by abiotic processes alone, then one can interpret this as evidence of a biological effect. Such an approach necessarily requires considerable sampling and is analytically intensive and expensive.

A second approach is morphology-specific, and relies on the assumption that larger precipitates (such as the larger needles from Grotta Bella) do not exchange measurably over long time scales. As such, the  $\delta^{44}\text{Ca}$  of the larger crystals are assumed to reflect the environment of the mineral at the time of precipitation with high fidelity. In this case, the objective of the approach is to determine whether  $\delta^{44}\text{Ca}$  variability in large crystals can be explained abiotically. The caveat to any application of such a biosignature, of course, is that a solution signal cannot be measured directly and, thus, a Ca source must be assumed based on the measurements of Ca sources in the system of interest. Ultimately, making the case for an isotopic biosignature is complex. Any single isotopic tool is likely to be ambiguous, and multiple tools are required. For this reason, we suggest Ca isotopes might prove a useful complement to other tools aimed at elucidating biosignatures.

## 5. CONCLUSIONS

In laboratory experiments, gypsum that precipitated in the presence of microbes at low pH had Ca isotopic compositions that were measurably lighter than abiotic precipitates. The biotic precipitates had irregular morphologies with smaller average aspect ratios relative to precipitates formed in the abiotic controls. We argue that this difference in growth is a consequence of selective inhibition by soluble and/or insoluble organic matter present in the biotic experiments. Although the microbial isotope effect observed in this study is small, it is consistent with Ca isotopic fractionation observed in gypsum from the Frasassi cave system. Our study of the Frasassi cave gypsum demonstrates the potential utility of Ca isotopes for elucidating the presence of microbes in the environment.

## ACKNOWLEDGEMENTS

M.S.F. acknowledges support from NSF grant EAR-0959092 and NASA grant NASA-NAI-NNA09DA76A (Penn State Astrobiology Center, PSARC). J.L.M acknowledges support from the National Science Foundation (NSF EAR-0525503) and NASA

grant NASA-NAI-NNA09DA76A (Penn State Astrobiology Center, PSARC). K.H. acknowledges a research assistantship support from PSARC, the NASA Earth and Space Science Graduate Fellowship (NESSF), and invaluable technical support from Ana Kolevica (GEOMAR) and Henry Gong, Julie Anderson, Denny Walizer, Karol Confer, Matthew Gonzales, Dr. Huimin Yu, and Dr. Scott Hynek (Penn State). K.H. appreciates valuable advice on Ca isotope measurements on the Neptune from Stephen Romaniello and Gwyneth Gordon at Arizona State University. The authors deeply appreciate the opportunity to conduct analyses in the laboratory of Dr. Anton Eisenhauer (GEOMAR), without whose generosity the Frasassi Ca isotope data would not have been collected. M.S.F. thanks Shaun Brown (Berkeley) profusely for his assistance with the gypsum analyses at the CIG, and Dr. Donald J. DePaolo for generously allowing access to the CIG facilities. The authors also thank Sandro Galdenzi for interesting and useful discussions of the caves and for providing samples. We also thank Alessandro Montanari (Osservatorio Geologico di Coldigioco) for laboratory space and logistical support during field work in Italy, and speleologists Sandro Mariani and Simone Cerioni for assistance in the field. Finally, the authors thank three anonymous reviewers and AE Jacobson for their constructive and detailed reviews, which improved the manuscript.

#### APPENDIX A. SUPPLEMENTARY DATA

Supplementary data associated with this article can be found, in the online version, at <http://dx.doi.org/10.1016/j.gca.2016.03.003>.

#### REFERENCES

- Allain P., Jaunault L., Mauras Y., Mermet J. and Delaporte T. (1991) Signal enhancement of elements due to the presence of carbon-containing compounds in inductively coupled plasma mass spectrometry. *Anal. Chem.* **63**, 1497–1498.
- Barcelona M. and Atwood D. (1978) Gypsum-organic interactions in natural seawater: effect of organics on precipitation kinetics and crystal morphology. *Mar. Chem.* **6**, 99–115.
- Barcelona M. and Atwood D. (1979) Gypsum-organic interactions in the marine environment: sorption of fatty acids and hydrocarbons. *Geochim. Cosmochim. Acta* **43**, 47–53.
- Barcelona M., Tosteson T. and Atwood D. (1976) Study of organic-calcium interactions: gypsum precipitation in tropical surface waters. *Mar. Chem.* **4**, 89–92.
- Blattler C. and Higgins L. (2014) Calcium isotopes in evaporites record variations in Phanerozoic seawater SO<sub>4</sub> and Ca. *Geology*. <http://dx.doi.org/10.1130/G35721>.
- Bosbach D. and Hochella M. (1995) Gypsum growth in the presence of growth inhibitors: a scanning force microscopy study. *Chem. Geol.* **132**, 227–236.
- Braissant O., Decho A., Dupraz C., Glunk C., Przekop K. and Visscher P. (2007) Exopolymeric substances of sulfate-reducing bacteria: interactions with calcium at alkaline pH and implication for formation of carbonate minerals. *Geobiology* **5**, 401–411.
- Cenki-Tok B., Chabaux F., Lemarchand D., Schmitt A. D., Pierret M. C., Viville D., Bagard M. L. and Stille P. (2009) The impact of water-rock interaction and vegetation on calcium isotope fractionation in soil- and stream waters of a small, forested catchment (the Strengbach case). *Geochim. Cosmochim. Acta* **73**, 2215–2228.
- Cobert F., Schmitt A., Calvaruso C., Turpault M., Lemarchand D., Collignon C., Chabaux F. and Stille P. (2011) Biotic and abiotic experimental identification of bacterial influence on calcium isotopic signatures. *Rapid Commun. Mass Spectrom.* **25**, 2760–2768.
- Cody R. (1991) Organo-crystalline interactions in evaporite systems: the effects of crystallization inhibition. *J. Sediment. Petrol.* **61**, 704–718.
- Cody A. and Cody R. (1989) Evidence for micro-biological induction of the 010 Montmartre twinning of gypsum (CaSO<sub>4</sub>·2H<sub>2</sub>O). *J. Cryst. Growth* **98**, 721–730.
- Cody A. and Cody R. (1991) Chiral habit modifications of gypsum from epitaxial-like adsorption of stereospecific growth inhibitors. *J. Cryst. Growth* **113**, 508–519.
- Collins K. (2006) Ion hydration: implications for cellular function, polyelectrolytes, and protein crystallization. *Biophys. Chem.* **119**, 271–281.
- Criss R. (1999) *Principles of Stable Isotope Distribution*. Oxford University Press, New York.
- De La Rocha C. L. and DePaolo D. J. (2000) Isotopic evidence for variations in the marine calcium cycle over the Cenozoic. *Science* **289**(5482), 1176–1178.
- DeOliveira D. and Laursen R. (1997) Control of calcite crystal morphology by a peptide designed to bind to a specific surface. *J. Am. Chem. Soc.* **119**, 10627–10631.
- DePaolo D. (2004) Calcium isotopic variations produced in biological, kinetic, radiogenic and nucleosynthetic processes. *Rev. Mineral. Geochem.* **55**, 255–288.
- DePaolo D. (2011) Surface kinetic model for isotopic and trace element fractionation during precipitation of calcite from aqueous solutions. *Geochim. Cosmochim. Acta* **75**, 1039–1056.
- Douglas T. and Mann S. (1994) Oriented nucleation of gypsum (CaSO<sub>4</sub>·2H<sub>2</sub>O) under compressed Langmuir monolayers. *Mater. Sci. Eng., C* **1**, 193–199.
- Dubois M., Gilles K. A., Hamilton J. K., Rebers P. A. and Smith F. (1956) Colorimetric method for determination of sugars and related substances. *Anal. Chem.* **28**, 350–356.
- DuVivier A., Jacobson A., Lehn G., Selby G., Hurtgen M. and Sageman B. (2015) Ca isotope stratigraphy across the Cenomanian-Turonian OAE 2: links between volcanism, seawater geochemistry, and the carbonate fractionation factor. *Earth Planet. Sci. Lett.* **416**, 121–131.
- Edinger S. (1973) The growth of gypsum: an investigation of the factors which affect the size and growth rates of the habit faces of gypsum. *J. Cryst. Growth* **18**, 217–224.
- Ewing S., Yang W., DePaolo D., Michalski G., Kendall C., Stewart B., Thiemens M. and Amundson R. (2008) Non-biological fractionation of stable Ca isotopes in soils of the Atacama Desert, Chile. *Geochim. Cosmochim. Acta* **72**, 1096–1110.
- Fantle M. S. (2010) Evaluating the Ca isotope proxy. *Am. J. Sci.* **310**, 194–230. <http://dx.doi.org/10.2475/03.2010.03>.
- Fantle M. and DePaolo D. (2007) Ca isotopes in carbonate sediment and pore fluid from ODP Site 807A: the Ca<sup>2+</sup> (aq)-calcite equilibrium fractionation factor and calcite recrystallization rates in Pleistocene sediments. *Geochim. Cosmochim. Acta* **71**, 2524–2546.
- Fantle M. and Higgins J. (2014) The effects of diagenesis and dolomitization on Ca and Mg isotopes in marine platform carbonates: implications for the geochemical cycles of Ca and Mg. *Geochim. Cosmochim. Acta* **142**, 458–481.
- Fantle M. and Tipper E. (2014) Calcium isotopes in the global biogeochemical Ca cycle: implications for development of a Ca isotope proxy. *Earth Sci. Rev.* **129**, 148–177.
- Farkaš J., Böhm F., Wallmann K., Blenkinsop J., Eisenhauer A., van Geldern R., Munnecke A., Voigt S. and Veizer J. (2007a) Calcium isotope record of Phanerozoic oceans: implications for chemical evolution of seawater and its causative mechanisms. *Geochim. Cosmochim. Acta* **71**, 5117–5134.

- Farkaš J., Buhl D., Blenkinsop J. and Veizer J. (2007b) Evolution of the oceanic calcium cycle during the late Mesozoic: evidence from  $\delta^{44/40}\text{Ca}$  of marine skeletal carbonates. *Earth Planet. Sci. Lett.* **253**, 96–111.
- Farkaš J., Déjeant A., Novák M. and Jacobsen S. B. (2011) Calcium isotope constraints on the uptake and sources of  $\text{Ca}^{2+}$  in a base-poor forest: a new concept of combining stable ( $\delta^{44}/42\text{Ca}$ ) and radiogenic ( $\epsilon\text{Ca}$ ) signals. *Geochim. Cosmochim. Acta* **75**(22), 7031–7046.
- Galdenzi S. (2012) Corrosion of limestone tablets in sulfidic ground-water: measurements and speleogenetic implications. *Int. J. Speleol.* **41**, 25–35.
- Galdenzi S. and Maruoka T. (2003) Gypsum deposits in the Frasassi caves, central Italy. *J. Cave Karst Stud.* **65**, 111–125.
- Gehrke T., Telegdi J., Thierry D. and Sand W. (2008) Importance of extracellular polymeric substances from *Thiobacillus ferrooxidans* for bioleaching. *Appl. Environ. Microbiol.* **64**, 2743–2747.
- Gonzales M. and Fantle M. S. (2014) Implications of  $\text{CaCO}_3$  phase heterogeneity for interpretation of the Ca isotopic fractionation factor: an in-situ study. Goldschmidt abstract.
- Griffith E., Fantle M., Eisenhauer A., Paytan A. and Bullen T. (2015) Effects of ocean acidification on the marine calcium isotope record at the Paleocene-Eocene Thermal Maximum. *Earth Planet. Sci. Lett.* **419**, 81–92.
- Grindlay G., Maestre S., Gras L. and Mora J. (2006) Introduction of organic solvent solutions into inductively coupled plasma-atomic emission spectrometry using a microwave assisted sample introduction system. *J. Anal. Atoms. Spectrom.* <http://dx.doi.org/10.1039/b606995a>.
- Grindlay G., Mora J., Loos-Vollebregt M. and Vanhaecke F. (2013) A systematic study on the influence of carbon on the behavior of hard-to-ionize elements in inductively coupled plasma-mass spectrometry. *Spectrochim. Acta Part B* **86**, 42–49.
- Gussone N., Eisenhauer A., Heuser A., Dietzel M., Bock B., Bohm F., Spero H., Lea D., Buma J. and Nagler T. (2003) Model for kinetic effects on calcium isotope fractionation ( $\delta^{44}\text{Ca}$ ) in inorganic aragonite and cultured planktonic foraminifera. *Geochim. Cosmochim. Acta* **67**, 1375–1382.
- Gussone N., Bohm F., Eisenhauer A., Dietzel M., Heuser A., Teichert B., Reitner J., Worheide G. and Dullo W. (2005) Calcium isotope fractionation in calcite and aragonite. *Geochim. Cosmochim. Acta* **69**, 4485–4494.
- Gussone N., Langer G., Geisen M., Steel B. and Riebesell U. (2007) Calcium isotope fractionation in coccoliths of cultured *Calcidiscus leptoporus*, *Helicosphaera carteri*, *Syracosphaera pulchra* and *Umbilicosphaera foliosa*. *Earth Planet. Sci. Lett.* **260**, 505–515.
- Gussone N., Bohm F., Nehrke G. and Teichert B. (2011) Calcium isotope fractionation in ikaite and vaterite. *Chem. Geol.* **285**, 194–202.
- Hamdona S. and Al Hadad U. (2007) Crystallization of calcium sulfate dihydrate in the presence of some metal ions. *J. Cryst. Growth* **299**, 146–151.
- Hamdona S. and Al Hadad O. (2008) Influence of additives on the precipitation of gypsum in sodium chloride solutions. *Desalination* **228**, 277–286.
- Harouaka K., Gonzales M., Eisenhauer A. and Fantle M. (2013) Using isotopic and morphological evidence to determine biogenicity of gypsum precipitates in the Frasassi Caves, Italy. *Mineral. Mag.* **77**, 1239–1351.
- Harouaka K., Eisenhauer A. and Fantle M. (2014) Experimental investigation of Ca isotopic fractionation during abiotic gypsum precipitation. *Geochim. Cosmochim. Acta* **129**, 157–176.
- Hazen R., Bekker A., Bish D., Bleeker W., Downs R., Farquhar F., Ferry J., Grew E., Knoll A., Papineau D., Ralph J., Sverjensky and Valley J. (2011) Needs and opportunities in mineral evolution research. *Am. Mineral.* **96**, 953–963.
- Heuser A. and Eisenhauer A. (2010) A pilot study on the use of natural calcium isotope ( $^{44}\text{Ca}/^{40}\text{Ca}$ ) fractionation in urine as a proxy for the human body calcium balance. *Bone* **46**, 889–896. <http://dx.doi.org/10.1016/j.bone.2009.11.037>.
- Heuser A., Eisenhauer A., Gussone N., Bock B., Hansen B. and Nagler T. (2002) Measurement of calcium isotopes ( $\text{d}^{44}\text{Ca}$ ) using a multicollector TIMS technique. *Int. J. Mass Spectrom.* **220**, 387–399.
- Hinojosa J. L., Brown S. T., Chen J., DePaolo D. J., Paytan A., Shen S. Z. and Payne J. L. (2012) Evidence for end-Permian ocean acidification from calcium isotopes in biogenic apatite. *Geology* **40**(8), 743–746.
- Holmden C. and Bélanger N. (2010) Ca isotope cycling in a forested ecosystem. *Geochim. Cosmochim. Acta* **74**(3), 995–1015.
- Horowitz E., McAlister D., Bond A. and Barrans R. (2005) Novel extraction of chromatographic resins based on tetraalkyldiglycoamides: characterization and potential applications. *Solvent Extr. Ion Exch.* **23**, 319–344.
- Jones D. (2013) Microbial ecology and biogeochemistry of sulfidic karst ecosystems. Ph.D. dissertation, Penn State University, University Park.
- Jones G. and Starkey R. (1961) Surface-active substances produced by *Thiobacillus thiooxidans*. *J. Bacteriol.* **82**, 788.
- Jones D., Lyon E. and Macalady J. (2008) Geomicrobiology of biovermiculations from the Frasassi Cave System, Italy. *J. Cave Karst Stud.* **70**, 78–93.
- Jones D., Schaperdoth I. and Macalady J. (2011) *Biogeography of Acidithiobacillus Populations in Extremely Acidophilic Subaerial Cave Biofilms* Dissertation. Pennsylvania State University, University Park, Pennsylvania.
- Jones D., Polerecky L., Galdenzi S., Dempsey B. and Macalady J. (2015) Fate of sulfide in the Frasassi cave system and implications for sulfuric acid speleogenesis. *Chem. Geol.* **410**, 21–27.
- Jost A. B., Mundil R., He B., Brown S. T., Altiner D., Sun Y., DePaolo D. J. and Payne J. L. (2014) Constraining the cause of the end-Guadalupian extinction with coupled records of carbon and calcium isotopes. *Earth Planet. Sci. Lett.* **396**, 201–212.
- Kasemann S. A., von Strandmann P. A. P., Prave A. R., Fallick A. E., Elliott T. and Hoffmann K. H. (2014) Continental weathering following a Cryogenian glaciation: evidence from calcium and magnesium isotopes. *Earth Planet. Sci. Lett.* **396**, 66–77.
- Krause S., Liebetrau V., Gorb S., Sánchez-Román M., McKenzie J. A. and Treude T. (2012) Microbial nucleation of Mg-rich dolomite in exopolymeric substances under anoxic modern seawater salinity: new insight into an old enigma. *Geology* **40**(7), 587–590.
- Langer G., Gussone N., Nehrke G., Riebesell U., Eisenhauer A. and Thoms S. (2007) Calcium isotope fractionation during coccolith formation in *Emiliana huxleyi*: independence of growth and calcification rate. *Geochem. Geophys. Geosyst.* **8**, 1–11.
- Lemarchand D., Wasserburg G. and Papanastassiou D. (2004) Rate-controlled calcium isotope fractionation in synthetic calcite. *Geochim. Cosmochim. Acta* **68**, 4665–4678.
- Macalady J., Jones D. and Lyon E. (2007) Extremely acidic, pendulous cave wall biofilms from the Frasassi cave system, Italy. *Environ. Microbiol.* **9**, 1402–1414.
- McMurry J. (2004) *Organic Chemistry*, sixth ed. Thomson-Brooks/Cole, ISBN 0534389996.
- Nielsen L., DePaolo D. and DeYoreo J. (2012) Self-consistent ion-by-ion growth model for kinetic isotopic fractionation during calcite precipitation. *Geochim. Cosmochim. Acta* **86**, 166–181. <http://dx.doi.org/10.1016/j.gca.2012.02.009>.

- Norris V., Chen M., Goldberg M., Voskuil J., McGurk G. and Holland B. (1991) Calcium in bacteria: a solution to which problem? *Mol. Microbiol.* **5**, 775–778.
- Page B., Bullen T. and Mitchell M. (2008) Influences of calcium availability and tree species on Ca isotope fractionation in soil and vegetation. *Biogeochemistry* **88**, 1–13.
- Parkhurst D. L., Appelo C. A. J., and U.S.G.S. (1999) User's guide to PHREEQC (version 2): a computer program for speciation, batch-reaction, one-dimensional transport, and inverse geochemical calculations. U.S. Geological Survey: Earth Science Information Center, Open-File Reports Section [distributor], Denver CO.
- Payne J. L., Turchyn A. V., Paytan A., DePaolo D. J., Lehrmann D. J., Yu M. and Wei J. (2010) Calcium isotope constraints on the end-Permian mass extinction. *Proc. Natl. Acad. Sci.* **107** (19), 8543–8548.
- Pourmand A. and Dauphas N. (2010) Distribution coefficients of 60 elements on TODGA resin: application to Ca, Lu, Hf, U and Th isotope geochemistry. *Talanta*. <http://dx.doi.org/10.1016/j.talanta.2010.01.008>.
- Reynard L., Day C. and Henderson G. (2011) Large fractionation of calcium isotopes during cave-analogue calcium carbonate growth. *Geochim. Cosmochim. Acta* **75**, 3726–3740.
- Riding R. and Awramik S. (2000) *Microbial Sediments*. Springer, ISBN 3-540-61828-7.
- Rouchy J. and Monty C. (2000) *Gypsum microbial sediments: neogene and modern examples*. *Microbial Sediments*. Springer-Verlag, Berlin Heidelberg New York, ISBN 3-540-61828-7, 209–216.
- Schmitt A., Vigier N., Lemarchand D., Millot R., Stille P. and Chabaux F. (2012) Processes controlling the stable isotope compositions of Li, B, Mg and Ca in plants, soils and waters: a review. *C.R. Geosci.* **344**, 704–722.
- Shock E. L. (1990) Geochemical constraints on the origin of organic compounds in hydrothermal systems. *Orig. Life Evol. Biosph.* **20**, 331–367.
- Shultze-Lam S., Fortin D., Davis B. and Beveridge T. (1996) Mineralization of bacterial surfaces. *Chem. Geol.* **132**, 171–181.
- Skulan J. and DePaolo D. J. (1999) Calcium isotope fractionation between soft and mineralized tissues as a monitor of calcium use in vertebrates. *Proc. Natl. Acad. Sci.* **96**(24), 13709–13713.
- Skulan J., DePaolo D. J. and Owens T. L. (1997) Biological control of calcium isotopic abundances in the global calcium cycle. *Geochim. Cosmochim. Acta* **61**(12), 2505–2510.
- Sutherland I. (2001) Biofilm exopolysaccharides: a strong and sticky framework. *Microbiology* **147**, 3–9.
- Tang J., Dietzel M., Bohm F., Kohler S. and Eisenhauer A. (2008) Sr<sup>2+</sup>/Ca<sup>2+</sup> and <sup>44</sup>Ca/<sup>40</sup>Ca fractionation during inorganic calcite formation: II. Ca isotopes. *Geochim. Cosmochim. Acta* **72**, 3733–3745.
- Tang J., Niedermayr A., Kohler S., Bohm F., Kisakurek B., Eisenhauer A. and Dietzel M. (2011) Sr<sup>2+</sup>/Ca<sup>2+</sup> and <sup>44</sup>Ca/<sup>40</sup>Ca fractionation during inorganic calcite formation: III. Impact of salinity/ionic strength. *Geochim. Cosmochim. Acta* (Manuscript number W8096).
- Tipper E. T., Galy A. and Bickle M. J. (2006) Riverine evidence for a fractionated reservoir of Ca and Mg on the continents: implications for the oceanic Ca cycle. *Earth Planet. Sci. Lett.* **247**(3), 267–279.
- Tipper E. T., Gaillardet J., Galy A., Louvat P., Bickle M. J. and Capmas F. (2010) Calcium isotope ratios in the world's largest rivers: a constraint on the maximum imbalance of oceanic calcium fluxes. *Glob. Biogeochem. Cycles* **24**(3).
- Uroz S., Calvaruso C., Turpault M. and Klett P. (2009) Mineral weathering by bacteria: ecology, actors and mechanisms. *Trends Microbiol.* **17**, 378–387.
- Vogel M., Des Maris S., Turk K., Parenteau M., Jahnke L. and Kubo M. (2009) The role of biofilms in the sedimentology of actively forming gypsum deposits at Guerrero Negro, Mexico. *Astrobiology* **9**, 875–893.
- Wang X. and Lee C. (1993) Adsorption and desorption of aliphatic amines, amino acids and acetate by clay minerals and marine sediments. *Mar. Chem.* **44**, 1–23.
- Yates K. and Robbins L. (1999) Radioisotope tracer studies of inorganic carbon and Ca in microbially derived CaCO<sub>3</sub>. *Geochim. Cosmochim. Acta* **63**, 129–136.

Associate editor: Andrew D. Jacobson